Cell

Article

Fertilization triggers early proteomic symmetry breaking in mammalian embryos

Graphical abstract

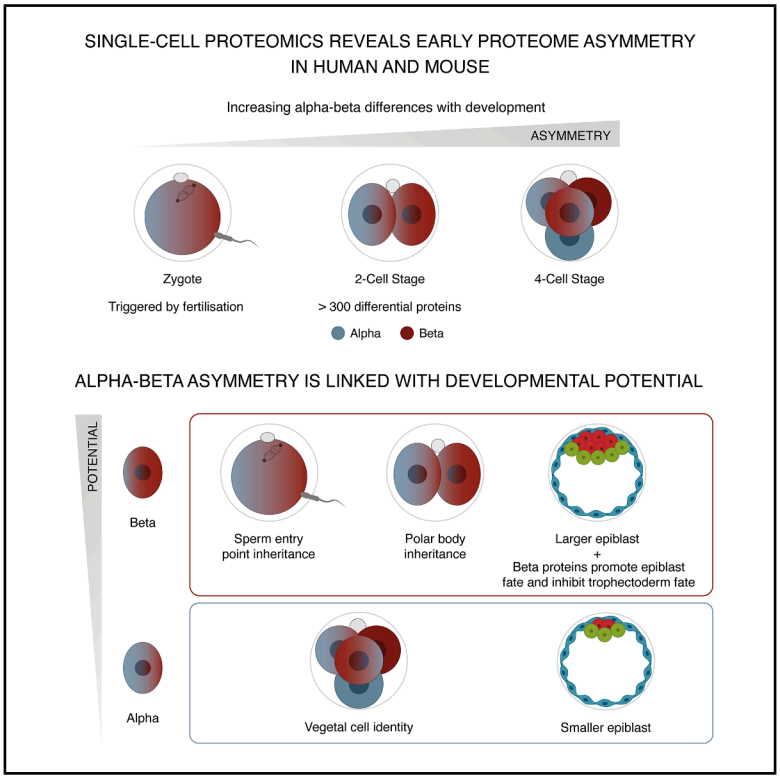

Highlights

- Proteomic asymmetries emerge at the zygote stage and are triggered by fertilization
- 2-cell-stage blastomeres cluster into alpha and beta states with unique profiles
- Beta blastomeres show greater developmental potential than alpha blastomeres
- Early asymmetries are conserved in human embryos

Authors

Lisa K. Iwamoto-Stohl, Aleksandra A. Petelski, Baiyi Quan, ..., Tsui-Fen Chou, Nikolai Slavov, Magdalena Zernicka-Goetz

Correspondence

magdaz@caltech.edu (M.Z.-G.), nslavov@northeastern.edu (N.S.), tfchou@caltech.edu (T.-F.C.)

In brief

Single-cell proteomics finds asymmetries between sister blastomeres from the 2-cell stage in human and mouse embryos, defining two states: alpha and beta. Alpha-beta asymmetry can be traced back to the zygote, is triggered by fertilization, and is linked to differential developmental potential, with beta blastomeres having a higher potential.

Iwamoto-Stohl et al., 2025, Cell *188*, 7428–7444
December 24, 2025
https://doi.org/10.1016/j.cell.2025.11.006

CellPress

CellPress
OPEN ACCESS

Cell

Article

Fertilization triggers early proteomic symmetry breaking in mammalian embryos

Lisa K. Iwamoto-Stohl,[1,2,7] Aleksandra A. Petelski,[3,4,7] Baiyi Quan,[2] Maciej Meglicki,[1] Audrey Fu,[1] Shoma Nakagawa,[2] Breanna McMahon,[2] Ting-Yu Wang,[2] Saad Khan,[3] Harrison Specht,[3,4] Gray Huffman,[3] Jason Derks,[3,4] Sergi Junyent,[2] Bailey A.T. Weatherbee,[1] Antonia Weberling,[5] Carlos W. Gantner,[1] Rachel S. Mandelbaum,[6] Richard J. Paulson,[6] Lisa Lam,[6] Tsui-Fen Chou,[2,8,*] Nikolai Slavov,[3,4,8,*] and Magdalena Zernicka-Goetz[1,2,8,9,*]

[1]Department of Physiology, Development and Neuroscience, University of Cambridge, Downing Street, Cambridge CB2 3DY, UK
[2]Division of Biology and Biological Engineering, California Institute of Technology (Caltech), Pasadena, CA 91125, USA
[3]Department of Bioengineering and Barnett Institute, Northeastern University, Boston, MA 02115, USA
[4]Parallel Squared Technology Institute, Watertown, MA 02472, USA
[5]Department of Biochemistry, University of Cambridge, Hopkins Building, Tennis Court Road, Cambridge CB2 1QW, UK
[6]Division of Reproductive Endocrinology and Infertility, Department of Obstetrics and Gynecology, University of Southern California, Los Angeles, CA, USA
[7]These authors contributed equally
[8]Senior author
[9]Lead contact
*Correspondence: magdaz@caltech.edu (M.Z.-G.), nslavov@northeastern.edu (N.S.), tfchou@caltech.edu (T.-F.C.)
https://doi.org/10.1016/j.cell.2025.11.006

SUMMARY

While non-mammalian embryos often rely on spatial pre-patterning, mammalian development has long been thought to begin with equivalent blastomeres. However, emerging evidence challenges this. Here, using multiplexed and label-free single-cell proteomics, we identify over 300 asymmetrically abundant proteins—many involved in protein degradation and transport—dividing mouse 2-cell-stage blastomeres into two distinct clusters, which we term alpha and beta. These proteomic asymmetries are detectable as early as the zygote stage, intensify by the 4-cell stage, and correlate with the sperm entry site, implicating fertilization as a symmetry-breaking event. Splitting 2-cell-stage embryos into halves reveals that beta blastomeres possess greater developmental potential than alpha blastomeres. Similar clustering and protein enrichment patterns found in human 2-cell embryos suggest this early asymmetry might be conserved. These findings uncover a previously unrecognized proteomic pre-patterning triggered by fertilization in mammalian embryos, with important implications for understanding totipotency and early lineage bias.

INTRODUCTION

In mammals, the fertilized egg undergoes a series of cleavage divisions that give rise to both embryonic and extraembryonic cell types.[1,2] Two successive fate decisions are crucial for blastocyst formation: the first segregates the outer cells, which differentiate into trophectoderm (TE), from the inner cell mass (ICM), while the second subdivides the ICM into epiblast and primitive endoderm (Figure 1A).[3,4]

For decades, it was thought that all blastomeres remain developmentally equivalent—and thus equally potent to give rise to all lineages, at least until the 16-cell stage.[5–7] This view has since evolved. Growing evidence now indicates that totipotency is gradually—and unequally—lost among blastomeres well before overt lineage specification.[2,8–13] In mice, lineage tracing reveals that the sister blastomeres of the 2-cell embryo contribute unequally to the embryonic and extraembryonic lineages.[9,14,15] Moreover, splitting 2-cell embryos into monozygotic "half embryos" reveals that while one blastomere can generate a viable embryo, the other typically cannot.[8,16] Similar asymmetries are seen in humans: clonal analyses of somatic mutations to infer lineages across tissues indicate that early blastomeres contribute unevenly to the embryo proper and placenta.[13,17–21] Direct lineage tracing in human embryos further supports this, showing that the majority of the epiblast typically arises from only one of the 2-cell blastomeres, while both contribute to the extraembryonic tissues.[9] Despite these insights, the molecular basis of this early asymmetry remains elusive.

In species like *Drosophila melanogaster*, symmetry breaking is driven by asymmetric mRNA localization, leading to unequal protein distribution and divergent cell fates.[22–25] In mammals, single-cell RNA sequencing has revealed transcript-level differences between blastomeres,[26–28] including the non-coding RNA LincGET at the 2-cell stage[29] and Sox21 at the 4-cell stage.[12] However, such RNA-level asymmetries are not consistently observed across embryos,[30] and transcript abundance

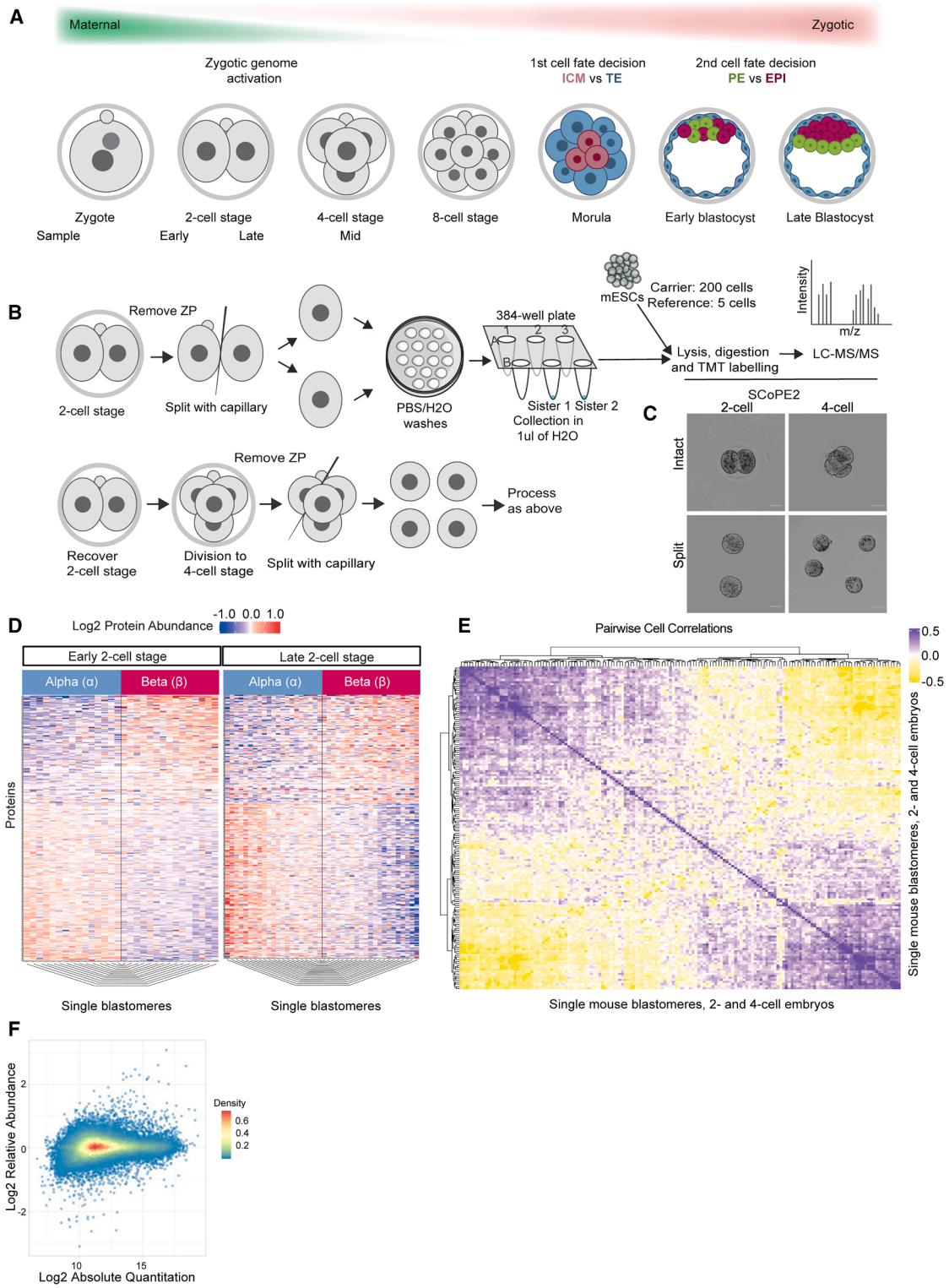

Figure 1. Proteomic asymmetry at the 2- and 4-cell-stage mouse embryos

(A) Schematic of pre-implantation development. Following a series of cleavage divisions, the embryo polarizes at the 8-cell stage and undergoes asymmetric and symmetric divisions to give rise to the inner cell mass (ICM) and outer trophectoderm (TE, blue) cells. The ICM then gives rise to the epiblast (EPI, magenta) and primitive endoderm (PE, green). Samples were collected at the early 2-cell stage (30–32 h post human chorionic gonadotrophin [hCG]), late 2-cell stage (46–48 h post hCG), and mid 4-cell stage (55–57 h post hCG).

(legend continued on next page)

does not always correlate with protein levels either across tissues[31] or during development.[32]

Whether proteomic differences exist between individual blastomeres of mammalian embryos remains largely unknown. In other models, such as *Xenopus laevis*, single-cell mass spectrometry (MS) has revealed proteomic asymmetries between early blastomeres within embryos,[33,34] and similar approaches have been used to profile human oocytes.[35] In mice, however, proteomic studies have thus far relied on bulk MS, which obscures cell-to-cell heterogeneity.[36–38]

Here, we use single-cell multiplexed and label-free MS to examine proteomic differences between individual blastomeres in both mouse and human embryos. We uncover striking proteome asymmetries as early as the zygote and 2-cell stages, revealing two reproducible proteomic states for blastomeres, which we designate alpha and beta, that distinguish sister cells within the same embryo. Importantly, these early proteome differences were predictive of the developmental potential of blastomeres and are correlated with the site of sperm entry during fertilization. Our findings provide a single-blastomere whole-proteome dataset for both mouse and human early embryos, revealing a previously unrecognized proteomic pre-patterning triggered by fertilization. This pre-patterning is linked to differences in developmental potential, offering insights into the molecular origins of symmetry breaking, cell fate bias, and the loss of totipotency.

RESULTS

Proteomic asymmetry in blastomeres of 2-cell- and 4-cell-stage embryos

To investigate early proteomic asymmetries, we wished to analyze individual sister blastomeres from (1) early 2-cell embryos, prior to the major wave of zygotic genome activation (ZGA); (2) late 2-cell embryos, during ZGA[39]; and (3) 4-cell embryos (Figures 1A–1C). To this aim, we developed a protocol to isolate and serially wash each blastomere from individual embryos, ensuring removal of protein contaminants from culture media while preserving the pairing of sister blastomeres (Figures 1B and 1C).

For protein quantification, we employed multiplexed single-cell proteomics MS (SCoPE2).[40,41] While an isobaric carrier composed of bulk blastomeres would have been ideal, this was impractical due to the number of blastomeres required. Instead, we used mouse embryonic stem cells (ESCs), which are derived from the ICM and available in large numbers, as carrier material. Carriers differing from the single-cell samples do not impact quantification,[42] and ESCs provide sufficient material for robust proteomic analysis. Proteins enriched in single cells but absent in the carrier can still be confidently detected, as confirmed by our dataset.

To determine proteomic differences between individual 2-cell blastomeres, we normalized protein abundance data from each individual blastomere to the mean expression within each embryo and performed k-means clustering. This revealed two distinct and consistent clusters, which we designated alpha and beta (Figure S1A). Remarkably, in all 36 2-cell embryos analyzed (15 early and 21 late 2-cell stage), sister blastomeres consistently segregated into opposite clusters, with each embryo containing one alpha and one beta blastomere, with high classification confidence (Figures 1D and S1B).

We identified 349 proteins that differed significantly in abundance between alpha and beta blastomeres (false discovery rate [FDR] < 1%), from an average of 1,043 proteins quantified per blastomere (Figure 1D; Table S1). These included maternal factors known to play a role in ZGA (e.g., the cortical granule protein Padi6[43–45] and the ubiquitin E3 ligase RNF114[46,47]) and cytoskeletal regulators later involved in TE specification (e.g., Rdx[48] and Cdc42[49,50]). To our knowledge, this represents the first systematic evidence of proteomic asymmetry between sister blastomeres in the 2-cell mouse embryo.

Proteomic differences between blastomeres increased in magnitude from early to late 2-cell stages, as shown by the intensified color scale in the heatmap (Figure 1D). Importantly, the overall variability in peptide quantification for the same proteins within each blastomere was low (Figure S1C) and did not correlate with the degree of asymmetry. There was also no correlation between differential and absolute protein abundance (Figure 1F), supporting the conclusion that these differences are biological rather than technical in origin.

We also analyzed 21 4-cell embryos, a stage when sister blastomeres are known to exhibit molecular and developmental heterogeneity.[10–12,51–54] Again, we observed two clusters (Figure 1E), and proteomic asymmetry persisted across embryos with variation in the magnitude of these differences (Figures S1D and S1E).

2-cell embryos reach the 4-cell stage via four distinct cleavage patterns, defined by the division orientation (meridional: along the animal-vegetal axis or equatorial: perpendicular to this axis) and the sequence of these divisions (Figure S2A). Previous

(B) Schematic showing the experimental harvesting of single blastomeres from 2-cell- (top) and 4-cell-stage (bottom) embryos for single-cell proteomics analysis. Following zona pellucida (ZP) removal, sister blastomeres were separated and washed before being collected for SCoPE2, with mESCs as carrier material.
(C) Representative images of embryos prior to and following splitting into individual blastomeres. Scale bars, 40 μm.
(D) K-means clustering of 2-cell-stage blastomeres results in consistent biclustering of sister blastomeres. Sisters from the same embryo fall into opposing clusters, which we term alpha and beta. Heatmaps of the 349 proteins with differential abundance in alpha and beta cells. $n = 72$ blastomeres from 15 early and 21 late 2-cell mouse embryos.
(E) Spearman correlation plot of all individual blastomeres from the 2- and 4-cell stages, which demonstrates the presence of two clusters. $n = 156$ blastomeres from 36 2-cell embryos and 31 4-cell embryos.
(F) A scatterplot showing the relationship between differential and absolute protein abundance in single blastomeres, where each point represents a protein. The absence of a relationship between relative and absolute abundances indicates consistent quantification across the dynamic range, suggesting measurement variance is not systematically dependent on signal intensity and that the applied normalization techniques are effective. Thus, the differences we observe between blastomeres are likely to reflect true biological variation, not measurement error and technical variability or noise.
See also Figures S1, S2, S3, and S7.

studies have shown that cleavage pattern can influence both molecular heterogeneity at the 4-cell stage[11] and overall developmental success.[10,51] To investigate whether these division patterns influence alpha-beta composition, we injected synthetic mCherry mRNA into one 2-cell blastomere, performed time-lapse imaging to track cleavage patterns, as previously described,[51,55] and then collected individual 4-cell blastomeres for SCoPE2 analyses (Figure S2B). Although we observed differences in some proteins and Gene Ontology (GO) terms between alpha and beta clusters depending on cleavage pattern, our sample size at this stage limited statistical power and precluded definitive conclusions (Figures S2C–S2F).

In summary, we identify robust, reproducible proteomic asymmetries among sister blastomeres in both 2- and 4-cell embryos. These differences define two molecular clusters—alpha and beta—revealing an early, conserved signature of asymmetry in mammalian development.

Proteomic asymmetry in the zygote

Having established alpha-beta proteomic asymmetry at the 2- and 4-cell stages, we next asked whether such asymmetries originate earlier, at the zygote stage. To test this, we manually bisected mouse zygotes meridionally along the animal-vegetal axis, the most common orientation of the first cleavage division.[55–57] While not all bisections align precisely with the natural cleavage plane due to the spherical geometry of the zygote, a subset will approximate the future cleavage plane (Figure 2A). We argued that if proteomic asymmetry is already established, we should expect that some zygote halves would exhibit alpha-beta-like differences. We collected and analyzed zygote halves by SCoPE2 (Figures 2A and 2B).

Using the same clustering approach as for 2-cell embryos, we found that zygote halves separate into two distinct clusters (Figure 2C). We then focused on a subset of 172 proteins that were quantified in zygote halves and differed significantly in abundance between alpha and beta 2-cell blastomeres (Table S1). Correlating the median fold changes of these proteins between zygote halves and between alpha versus beta 2-cell blastomeres revealed a significant correlation (Spearman $r = 0.45$, $p < 1e{-}8$; Figure 2D), suggesting that cluster 1 zygote halves resemble alpha blastomeres, while cluster 2 aligns with beta. Pairwise correlation analyses of protein fold changes between zygote halves and between 2-cell blastomeres confirmed that most zygote halves showed alpha-beta-like differences (a positive correlation), with the strength of this correlation scaled with PC1 separation (Figures 2C and 2E), likely reflecting how well the bisection captured the endogenous protein gradient. These findings indicate that proteomic asymmetry arises in the zygote and is propagated to the 2-cell stage.

Alpha and beta blastomeres are enriched for distinct biological processes

To investigate which biological processes differ between alpha and beta blastomeres, we performed protein set enrichment analysis (PSEA) for the early and late 2-cell stages. This revealed significant differences (q values < 0.05) in pathways related to protein transport, degradation, and translation (Figures S3A–S3C). Beta blastomeres were particularly enriched in protein transport terms, such as ion channels, signaling components, molecular motors, and vesicle trafficking. Notably, molecular motor-related processes exhibited the largest median fold differences (Figure S3B).

We also compared the proteome of single blastomeres to bulk carrier samples of 200 ESCs. Surprisingly, many peptides were up to 10-fold more abundant in single blastomeres than in the ESCs (Figure S3D). At first glance, this result was unexpected, as overall peptide abundance should correlate with sample size. However, these enriched peptides included components of the subcortical maternal complex, a maternally deposited multiprotein assembly critical for early development,[58] as well as ubiquitin ligase-associated proteins.

Further GO term enrichment analysis confirmed that single blastomeres were enriched for proteins involved in proteasomal degradation and transport, relative to ESCs (Figure S3E). This is consistent with the known importance of protein turnover and proteostasis in early embryogenesis, particularly during maternal protein clearance, the onset of ZGA, and the initiation of zygotic protein synthesis.[46,47,59–61] Many of these same pathways were differentially represented between alpha and beta blastomeres, suggesting a potential link between early proteome heterogeneity and distinct developmental trajectories.

Dynamics of alpha and beta differences

During the zygote and early 2-cell stages, before the onset of the major ZGA wave, mouse embryos rely heavily on maternally inherited cellular components—including proteins, mRNAs, and ribosomes. Previous studies have proposed that variations in ribosomal composition contribute to translational control during early embryogenesis[62,63] and in ESCs.[64,65] To explore this possibility, we examined the abundance of ribosomal proteins (RPs) in our single-blastomere proteomic dataset.

We found that most RPs were slightly but significantly more abundant in alpha blastomeres compared with beta blastomeres at the early 2-cell, late 2-cell, and 4-cell stages (Figure S3F). An exception was RPS27A, which showed progressive enrichment in beta blastomeres over time. Correspondingly, translation initiation factors were elevated in alpha blastomeres, whereas GO terms associated with the endoplasmic reticulum were enriched in beta blastomeres (Figure S3C), suggesting differences in translational regulation and protein processing pathways.

To assess how alpha and beta differences evolve over time, we calculated the Euclidean distances between alpha and beta blastomeres from the same embryo, using proteins quantified across all samples. Consistent with the heatmap in Figure 1D, the degree of proteomic differences between alpha and beta blastomeres increased over developmental time (Figure 2F), indicating progressive divergence between sister cells.

This divergence was primarily driven by proteins that showed either increasing or decreasing abundance in alpha and beta blastomeres over time. Of the 324 proteins that were differentially abundant between alpha and beta blastomeres at both the early and late 2-cell stages, 278 maintained consistent cluster identity and exhibited monotonic trends. When including the 4-cell stage, 254 proteins preserved their alpha or beta identity, with 108 showing continuous trajectories across all three stages (Figure 2G).

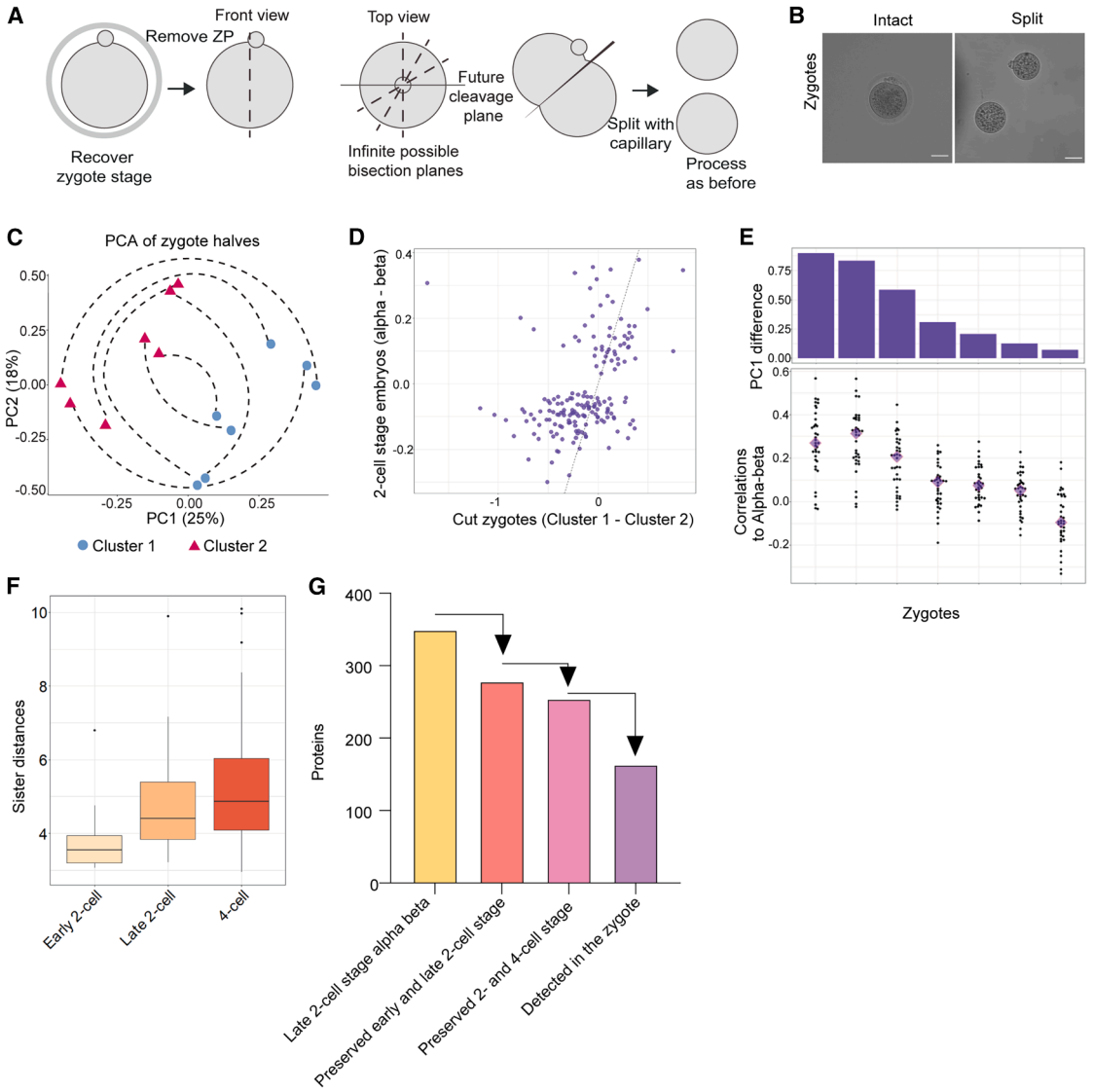

Figure 2. Proteomic asymmetry is inherited from the zygote and increases over subsequent development

(A) Schematic illustrating the collection of zygotes and subsequent meridional cutting. Following zona pellucida (ZP) removal, zygotes were cut along the animal-vegetal axis as defined by the position of the second polar body (PB).

(B) Representative images of zygotes prior to and following splitting into individual halves. Scale bars, 40 μm.

(C) Principal-component analysis (PCA) of the zygote halves shows a biclustering pattern. Each zygote half pair splits into separate clusters. $n = 14$ halves from 7 split zygotes.

(D) Scatterplot showing the correlation (0.45, $p = < 1e{-}8$) between the median protein fold changes for zygote halves (x axis) and the median protein fold changes for sister blastomeres at the 2-cell stage (y axis). Fold changes were calculated for proteins that were both differentially abundant between alpha and beta cells at the 2-cell stage and quantified in zygotes.

(E) Plots showing the relationship between PC1 loadings for each zygote pair (ordered in descending order, top) and the pairwise Spearman correlations between each zygote pair and the 2-cell-stage embryos (bottom). Correlations were computed on vectors of fold changes for proteins that were both significantly differential between alpha and beta cells and quantified in zygotes. Triangles indicate the median of each distribution.

(F) Euclidean distance of the normalized protein abundance between each blastomere in each embryo, showing increasing inter-blastomere differences with development (1% FDR).

(G) A bar plot showing the number of proteins (1) that were quantified in both early and late 2-cell embryos and were differentially abundant between alpha and beta blastomeres (yellow), (2) that preserved cluster identity and are either consistently increasing or decreasing over the 2-cell stage (red), (3) that continue to preserve cluster identity at the 4-cell stage (pink), and (4) that are monotonically changing across both the 2- and 4-cell stages (purple).

See also Figure S3.

To explore which biological processes are showing monotonic divergence, we performed PSEA using Spearman correlations across all three developmental stages and the corresponding protein fold changes between alpha and beta blastomeres from each embryo. We identified distinct trends: for example, beta blastomeres showed increasing enrichment for processes such as thioredoxin peroxidase activity and dATP binding, while alpha blastomeres showed progressive increases in pathways including proteasome regulatory particle activity, aspartate metabolism, and DNA helicase activity (Figures S3G and S3H).

The role of beta-enriched proteins in lineage fate

To investigate the functional relevance of proteins that are differentially abundant between alpha and beta blastomeres, we focused on three candidates: Nedd8, Gps1, and PSMC4. These were selected based on their marked differences in abundance (Tables S1, S2, and S3) and potential importance in early development. Nedd8, a ubiquitin-like protein, has been linked to ICM formation.[66] Gps1 (also known as Cops1) is part of the constitutive photomorphogenesis 9 (COP9) signalosome,[67] which is involved in deneddylation and has been implicated in maintaining naive pluripotency and supporting epiblast survival.[68–70] Although Gps1 is known to regulate Oct4 expression in human ESCs,[71] its role in mammalian embryos was previously unexplored. PSMC4, a 26S proteasome component, is essential for development up to the blastocyst stage.[72] Nedd8 and Gps1 were enriched in beta blastomeres, while PSMC4 was enriched in alpha blastomeres (Table S2).

To test the function of these proteins, we performed knockdowns by injecting double-stranded RNA (dsRNA) targeting each candidate gene (or eGFP as a control) into one blastomere of the 2-cell embryo, along with Gap43-RFP mRNA to label the progeny, following our established protocol[73,74] (Figure 3A). Embryos were cultured for 3 days until the blastocyst stage, fixed, and stained for lineage markers: Cdx2 (TE) and Sox17 (primitive endoderm; Figures 3A and 3B). Knockdown efficiency was validated by RT-qPCR 48 h post-injection (Figures S4A–S4D).

Nedd8 knockdown resulted in an increase in both total cell number and the proportion of RFP-positive cells compared with controls (Figures 3C and 3D). It also led to a higher contribution of RFP-positive cells to the TE lineage, with no significant effect on the epiblast or primitive endoderm (Figure 3E). These results suggest that Nedd8 may act to restrict TE specification or proliferation.

Gps1 knockdown had no effect on total cell number (Figure 3F) but reduced the contribution of RFP-positive cells, particularly to the epiblast, with milder effects on primitive endoderm and none on TE (Figures 3G and 3H). These findings indicate that Gps1 supports epiblast specification or proliferation, in line with its known pluripotency-promoting roles.[71]

PSMC4 knockdown led to reduced total cell number and a global reduction in the contribution of RFP-positive cells across all lineages (Figures S4E–S4H), consistent with its role in proteosome function and general impact on cell division.[59]

Together, these results validate the biological impact of alpha-beta proteins identified by SCoPE2. Nedd8 and Gps1—more abundant in beta blastomeres—influence TE and epiblast development, respectively. By contrast, PSMC4—enriched in alpha blastomeres—affects all lineages, likely reflecting its general importance in cellular homeostasis and proteostasis. These findings underscore the functional consequences of early proteome asymmetries during pre-implantation development.

Alpha and beta identity predict developmental potential

Previous studies, including our own, have shown that sister blastomeres at the 2-cell stage differ in developmental potential.[8–10,14–16,51,75] When 2-cell embryos are split to generate monozygotic "twin" embryos, only one typically forms a viable blastocyst, often with a larger epiblast compartment, indicating intrinsic asymmetry[8] (Figures S5A–S5C). To determine if alpha and beta identity predicts this differential potential, we separated sister blastomeres at the 2-cell stage. One sister was subjected to proteomic analysis using SCoPE2 or pSCoPE[76] to determine its identity (alpha or beta, as classified by the alpha-beta fold change; Figure S5D), while the other was cultured individually to the blastocyst stage (Figures 4A, 4B, S5E, and S5F). Since each embryo contains one alpha and one beta cell (Figure 1D), the identity of the cultured blastomere could be inferred from its sibling.

When we examined the lineage composition of the resulting blastocyst (Figures S5E–S5H), we found that beta blastomeres gave rise to blastocysts with a significantly higher proportion of epiblast cells, while alpha blastomeres generated blastocysts with fewer epiblast cells (Figure 4C). Moreover, beta blastomeres more frequently generated blastocysts with more than four epiblast cells—the minimum threshold known to be required for further development[51] (Figure 4D). These findings are consistent with our knockdown data, which showed that Gps1, a protein enriched in beta blastomeres, may promote epiblast formation.

Previous studies have shown that at the 2-cell stage, the blastomere that inherits the second polar body contributes to the ICM more.[77] Consistent with this, we found that the blastomere associated with the second polar body was significantly more likely to be classified as beta (Figure 4E).

Similarly, at the 4-cell stage, vegetal blastomeres—those positioned opposite the second polar body—are known to have reduced developmental potential.[10,51] We therefore examined the alpha-beta identity of vegetal blastomeres in our 4-cell-stage embryos (Figure 4F). Among embryos with clear alpha-beta polarization, vegetal blastomeres were significantly more likely to be classified as alpha (Figure 4F), further reinforcing the link between alpha identity and reduced developmental potential.

Finally, we investigated whether cell cycle asynchrony correlates with alpha-beta identity. To this end, we injected zygotes with proliferating cell nuclear antigen (PCNA)-clover mRNA to visualize S-phase progression[78,79] (Figures S6A and S6B). Embryos were split into individual blastomeres and imaged during the 2-cell stage, then analyzed by pSCoPE.[76] Although sister blastomeres again separated into alpha and beta clusters, we found no consistent relationship between S-phase exit timing and alpha-beta identity (Figure S6C). In a separate experiment, split embryos were cultured to the blastocyst stage following live imaging to assess S-phase progression, and no significant difference in epiblast cell number was observed based on S-phase timing (Figures S6D and S6E). These findings suggest

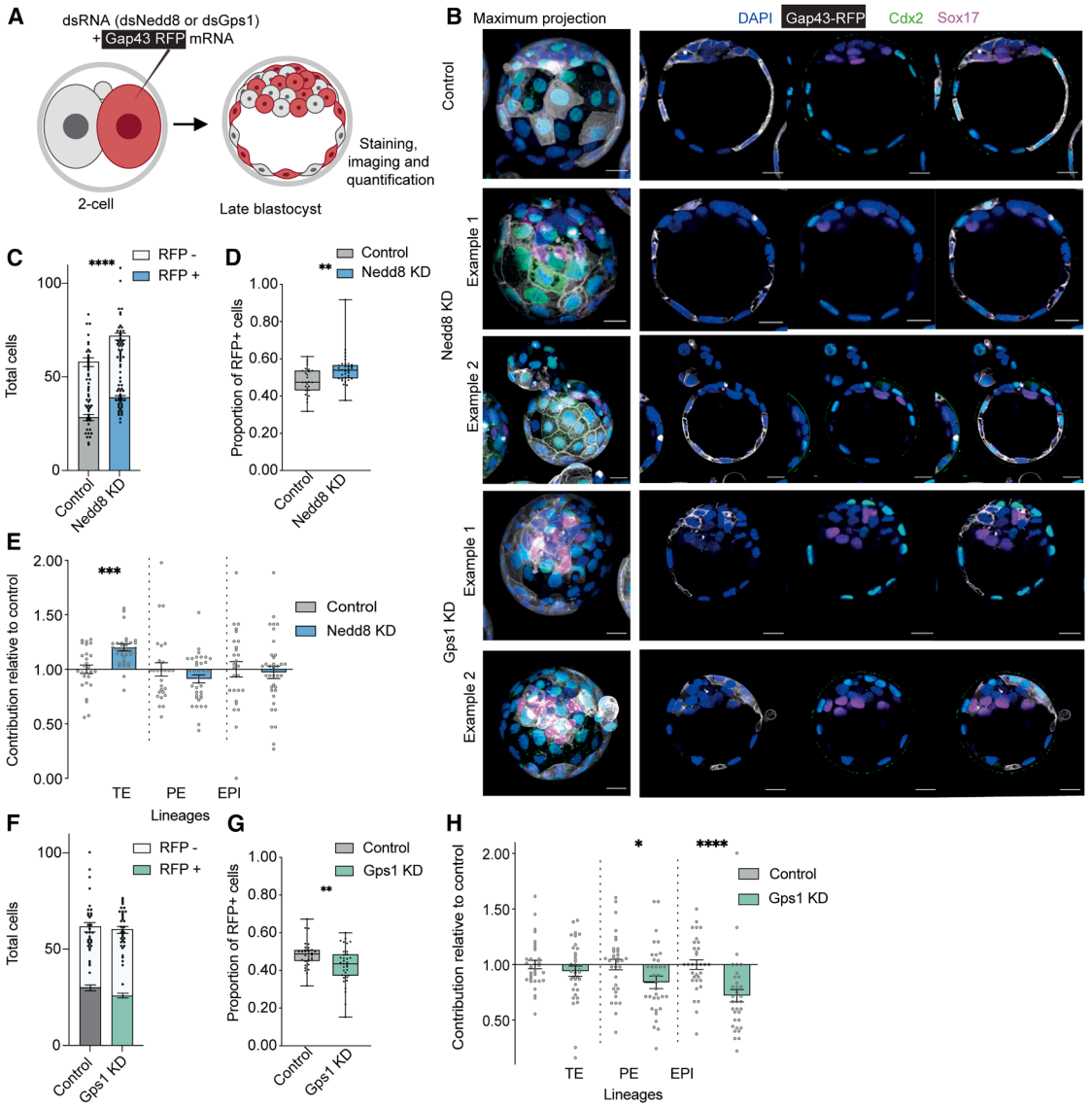

Figure 3. Manipulation of beta proteins impacts lineage composition

(A) Schematic of clonal dsRNA-mediated knockdown (KD) of candidates. One blastomere of 2-cell-stage embryos was injected with dsRNA targeting candidates (dsNedd8 or dsGps1) or eGFP (control) and mRNA for the membrane marker Gap43-RFP to mark the progeny of the cell. Embryos were cultured to the late blastocyst stage, and the contribution of the Gap43-RFP-positive cells to each lineage was analyzed.

(B) Representative images of control, dsNedd8, and dsGps1 blastocysts. Scale bar, 20 μm.

(C) Bar chart showing the average total number of cells and the number of RFP-positive or -negative cells in control and dsNedd8 late blastocysts. dsNedd8 blastocysts have significantly more cells in total than controls. Mann-Whitney test, $^{****}p < 0.0001$.

(D) Boxplot showing the RFP-positive proportion of total cells in each blastocyst. Increased contribution of dsNedd8 cells can be seen. Mann-Whitney test, $^{**}p = 0.0024$.

(E) Bar plot showing the contribution of RFP-positive cells to the trophectoderm (TE, Cdx2 positive), primitive endoderm (PE, Sox17 positive), and epiblast (EPI, double-negative), with dsNedd8 contribution assessed relative to controls. dsNedd8 cells show increased contribution to the TE lineage. Control, $n = 27$ embryos; dsNedd8, $n = 36$ embryos. Mann-Whitney test, $^{***}p = 0.0005$.

(F) Bar chart showing the average total number of cells and the number of RFP-positive or -negative cells in control and dsGPS1 late blastocysts.

(G) Boxplot showing the RFP-positive proportion of the total cells in each blastocyst. Decreased contribution of dsGps1 cells can be seen. Mann-Whitney test, $^{**}p = 0.0081$.

(H) Bar plot showing the contribution of RFP-positive cells to the TE, PE, and EPI. dsGps1 contribution was assessed relative to control embryos, and dsGps1 cells were found to have significantly reduced EPI contribution. Control, $n = 33$ embryos; dsGps1, $n = 35$ embryos. Mann-Whitney test, $^{*}p = 0.0274$, $^{****}p < 0.0001$.

For (C)–(H), data are shown as mean ± SEM.

See also Figure S4.

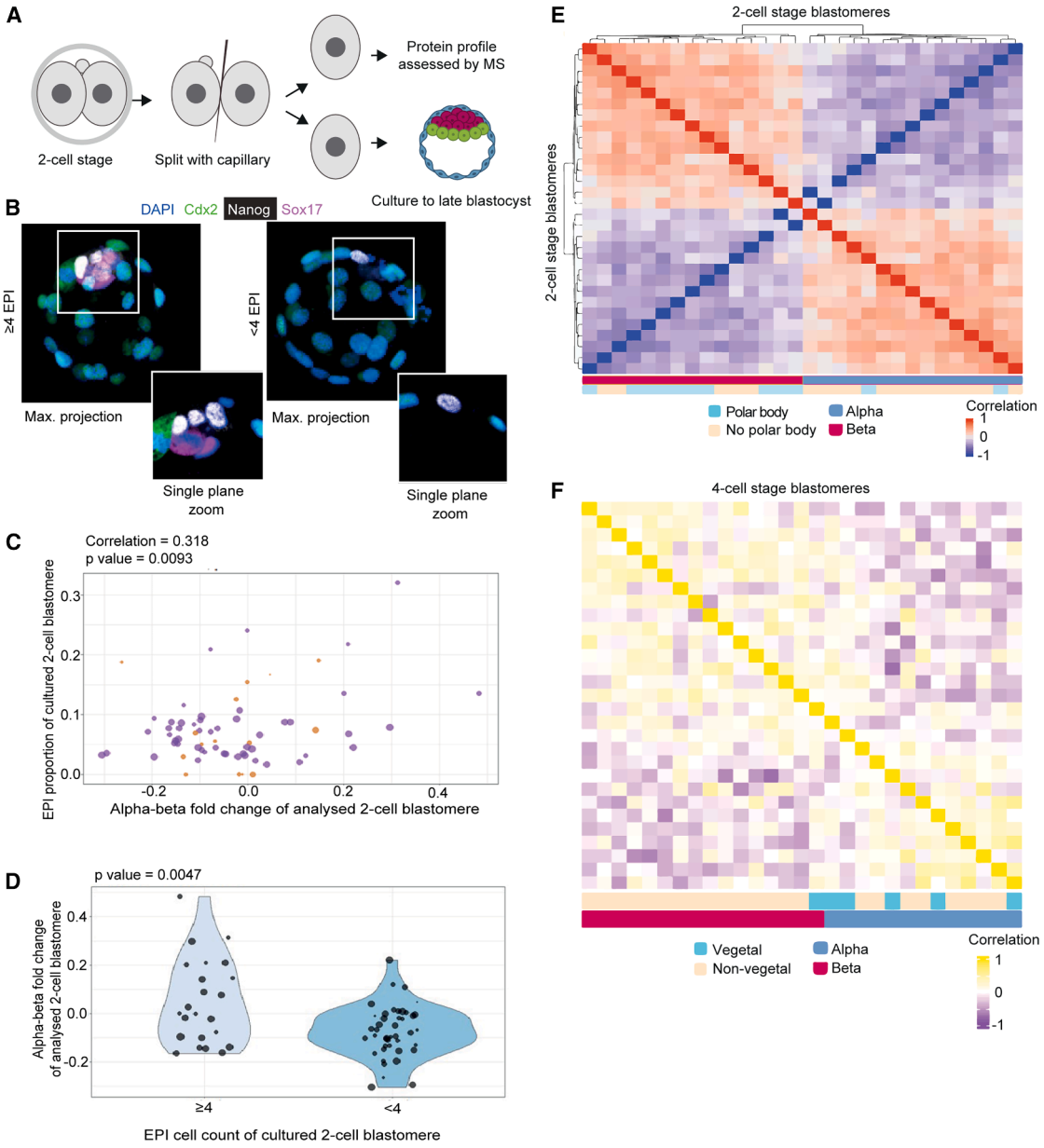

Figure 4. Beta and alpha blastomeres exhibit higher and lower developmental potential, respectively

(A) Schematic illustrating the experimental approach: one sister blastomere from the 2-cell embryo was collected for single-cell proteomics analysis, while the other was cultured to the blastocyst stage to assess developmental potential.

(B) Representative images of blastocysts with 4 or more epiblast (EPI) cells and fewer than 4 EPI cells. Images are shown as maximum projections and representative single-plane zooms showing the composition of the ICM.

(C) Normalized EPI cell counts positively correlate with sister cells' alpha-beta polarization. Plot showing paired blastomere data filtered to include only sister blastocysts with a minimum total of 10 cells and no more than one absent lineage. Point size indicates the total number of cells present in the resulting blastocyst derived from the cultured blastomere. Point color reflects lineage composition: purple indicates the presence of all three lineages, while brown indicates blastocysts with two lineages. A Pearson correlation was calculated across all datapoints to assess the relationship between EPI cell number and the alpha-beta polarization of the corresponding sister blastomere ($p = 0.0047$).

(D) Violin plots showing the alpha-beta polarization scores of sister 2-cell blastomeres paired to blastocysts developing from their corresponding sisters with either at least 4 EPI cells or fewer than 4 EPI cells. Only blastocysts containing more than 10 cells and no more than one missing lineage were included in this analysis ($n = 81$ blastocysts and paired 2-cell-stage blastomeres). Each data point represents a blastocyst, with point size proportional to the total blastocyst cell count. The two blastocyst groups showed a statistically significant difference in their paired sisters' alpha-beta polarization scores ($p = 0.005$, two-tailed t test).

(E) Heatmap showing the pairwise cell correlations for all early 2-cell-stage blastomeres. Correlations were calculated based on quantified alpha-beta proteins. Each tile represents a correlation value between two blastomeres, while the color bars indicate alpha or beta classification and whether the cell was associated with the PB. Cells that had the PB are more likely to cluster with beta cells ($p = 0.0036$, hypergeometric distribution probability test).

(legend continued on next page)

that alpha-beta identity is not determined by cell cycle asynchrony.

Together, these results demonstrate that alpha-beta identity is predictive of developmental potential, with beta blastomeres giving rise to more epiblast cells and showing higher developmental competence, while alpha blastomeres are associated with reduced potential.

Fertilization triggers the breaking of symmetry

The asymmetric distribution of proteins in the zygote could be maternally inherited, triggered by fertilization, or both. To determine whether proteome asymmetry arises independently of fertilization, we first analyzed the proteome of single sister blastomeres from 2-cell-stage parthenogenetic embryos, which develop in the absence of sperm contribution (Figure 5A). In striking contrast to fertilized embryos, MS revealed no clear clustering patterning and no consistent proteome asymmetry between sister 2-cell-stage blastomeres (Figure 5B). This result suggests that maternal factors alone are insufficient to generate the alpha-beta asymmetry observed in fertilized embryos.

To further investigate whether sperm entry contributes to symmetry breaking, we performed zygote-splitting experiments in which the fertilization cone—marking the site of sperm entry—was labeled with a microbead immediately after *in vitro* fertilization (IVF; Figures 5C and 5D), using our previously established protocol.[15,80] Zygotes were then bisected meridionally with respect to the animal pole, defined by the attachment of the second polar body, generating one-half that inherited the sperm entry site (bead-labeled) and one that did not. Each zygote half was subjected to proteomic analysis.

Remarkably, zygote halves inheriting the sperm entry point clustered together, forming a distinct group from the non-inheriting halves (Figures 5E and 5F). Moreover, the proteomic differences between fertilization cone-positive and -negative halves were significantly correlated with the proteomic differences observed between sister blastomeres at the 2-cell stage and alpha-beta identity (Figures 5G and 5H). This strongly suggests that fertilization triggers proteome asymmetry in the zygote, which is subsequently inherited by daughter blastomeres.

Finally, to assess whether inheritance of the sperm entry point predicts developmental outcome, we tracked the fate of individual 2-cell blastomeres in relation to inheritance of the sperm entry point. After IVF and fertilization cone labeling, 2-cell embryos were split into individual blastomeres, annotated for microbead inheritance, and cultured to the blastocyst stage (Figures 5I and 5J). Blastomeres that inherited the sperm entry point produced blastocysts with significantly higher epiblast cell proportions (Figure 5K), mirroring the developmental bias we observed for beta blastomeres.

Together, these results identify fertilization as a trigger for proteomic symmetry breaking in the zygote. This initial asymmetry is passed on to the daughter blastomeres, with the beta blastomere inheriting the sperm entry point and exhibiting higher developmental potential.

Proteome asymmetry is conserved in human 2-cell-stage embryos

We next asked whether the proteomic signatures that distinguish alpha and beta blastomeres in mice might be conserved in 2-cell human embryos (Figure 6A). Due to the scarcity of human embryos, our sample size was necessarily smaller than in mice. To maximize confidence, we employed two complementary single-cell MS methods: label-free data-independent acquisition (DIA) and multiplexed SCoPE2 data-dependent acquisition (DDA). These orthogonal approaches quantify peptides via different ion types—precursor ions for DIA and reporter ions for DDA—thus minimizing shared technical biases and increasing confidence in our findings.[81,82] DDA prioritizes the most abundant peptides from MS1 for MS2 fragmentation and sequential analysis, while DIA fragments all peptides within a defined mass/charge window simultaneously, generating complex composite spectra.

Using the same k-means clustering approach applied to mouse blastomeres, we found that sister blastomeres from human 2-cell embryos reliably segregated into two distinct clusters (Figure 6B). We identified 105 proteins that were differentially abundant between clusters at a 1% FDR (Figure 6C; Table S4). To validate these results, we examined the extracted ion chromatogram (XIC) for VDAC2—a voltage-dependent anion-selective channel protein with a high fold change—and confirmed consistent differential abundance between blastomeres across both the MS1 and the MS2 signals (Figure 6D). VDAC2 and other protein transport factors were also differentially enriched between mouse alpha and beta blastomeres, suggesting a conserved role.

To characterize the biological pathways represented in this proteomic asymmetry, we performed PSEA. As in mice, we observed enrichment for pathways related to protein degradation and transport (Figure 6E). Specifically, ubiquitin-related proteins were enriched in one cluster (cluster 1), while vesicle transport-associated proteins were enriched in the other (cluster 2), mirroring the mouse alpha and beta differences.

To directly assess conservation of these clusters across the two species, we analyzed the 877 orthologous proteins quantified in both human and mouse 2-cell embryos. Pairwise correlation analysis showed that the two human clusters aligned closely with the mouse alpha and beta profiles (Figure 7A), enabling cross-species annotation of human blastomeres as alpha or beta. GO enrichment patterns between mouse and human also displayed strong directional concordance (Figure 7B; Table S5), reinforcing the conservation of biological processes. At the level of individual proteins, we found that among the mouse alpha-beta differential proteins also detected in humans, 68 showed consistent fold-change direction across species, while 98 displayed opposite trends

(F) Heatmap of pairwise correlations between 4-cell-stage blastomeres based on vectors of alpha-beta proteins with a high fold change. Each tile represents a correlation value between two blastomeres. Color bars indicate each blastomere's alpha-beta classification and whether it was a vegetal cell. Two distinct clusters can be seen, corresponding to alpha and beta. Vegetal cells are significantly enriched within the alpha cluster ($p = 0.047$, hypergeometric distribution probability test), suggesting a relationship between vegetal identity and alpha polarization.
See also Figures S5 and S6.

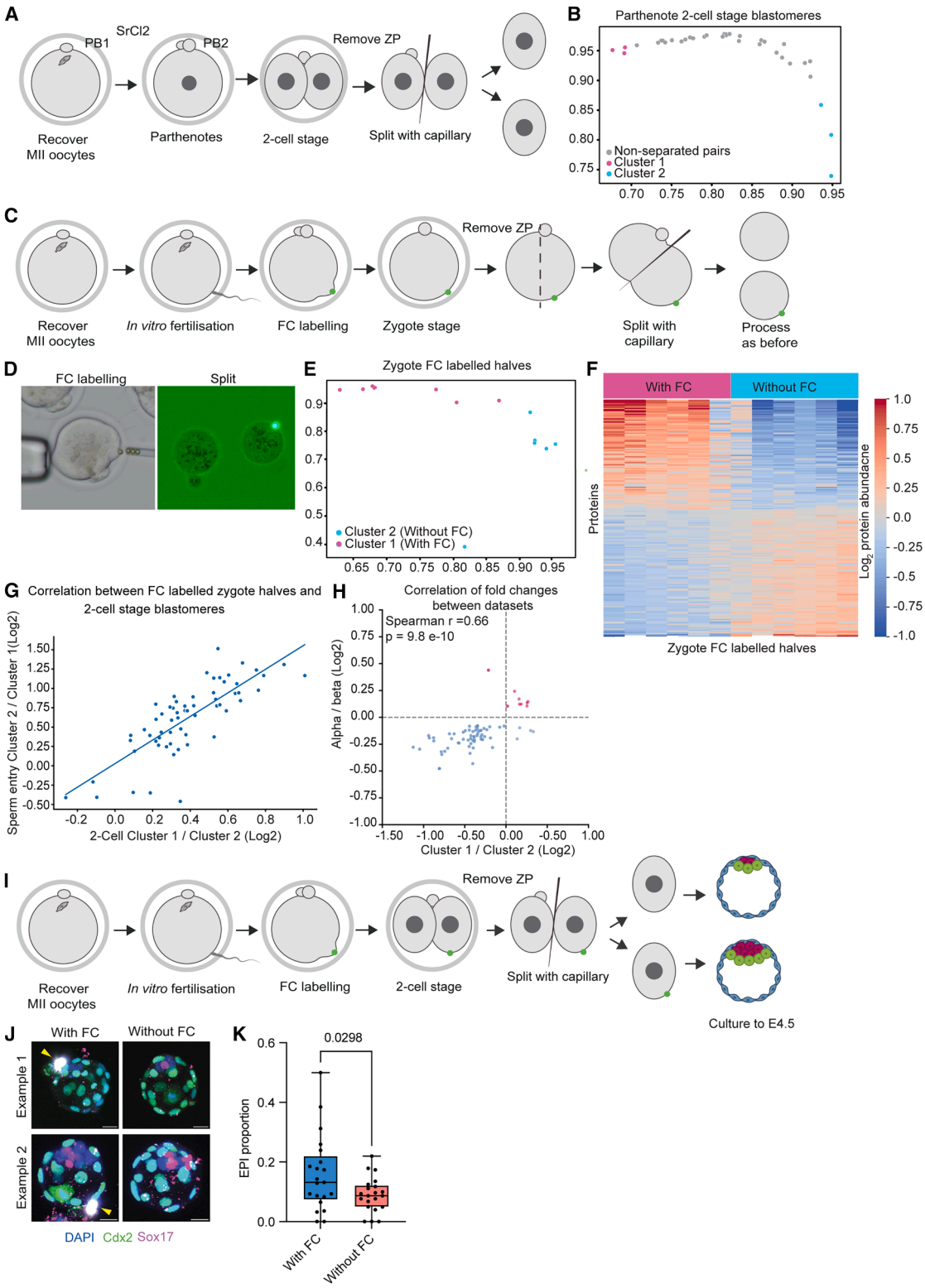

Figure 5. Proteomic asymmetry is triggered by fertilization

(A) A schematic showing the experimental harvesting of single blastomeres from parthenogenetic 2-cell embryos for single-cell proteomics. SrCl2, strontium chloride; ZP, zona pellucida; PB, polar body.

(B) K-means clustering of parthenogenetic 2-cell-stage blastomeres. The majority of pairs did not split across clusters and are labeled "non-separated pairs."

(legend continued on next page)

(Figures 7C and 7D). This suggests that although the core biological processes are conserved, species-specific regulatory differences exist for individual proteins.

In summary, these findings provide compelling evidence that proteome asymmetry between sister blastomeres is a conserved feature of early mammalian development, detectable at both the individual protein and pathway level in mouse and human embryos.

DISCUSSION

For decades, it was assumed that all blastomeres of mouse and human embryos were developmentally equivalent until they acquired differential positions within the embryo at the 8–16-cell stage transition. Yet, advances in live-cell tracing of individual blastomeres in living embryos and single-cell transcriptomics have revealed that differences between blastomeres emerge much earlier in development.[9,10,12,29,51,80] Strikingly, when 2-cell-stage mouse embryos are split into individual blastomeres, often only one sister proves truly totipotent,[8,16] suggesting that symmetry is broken before positional cues appear. What then accounts for this early asymmetry? In this study, we applied single-cell MS-based proteomics to map intra-embryonic differences from the zygote to the 4-cell stage in normally fertilized and parthenogenetically activated embryos.

We identified striking asymmetries in protein abundance between sister blastomeres, emerging as early as the zygote stage and persisting through the 2- and 4-cell stages. In 2-cell mouse embryos, blastomeres consistently separated into two distinct clusters, which we termed alpha and beta. This proteomic dichotomy was also evident in human 2-cell embryos, where similar biclustering was observed.

Generating and processing these samples posed considerable technical challenges. We developed and optimized a protocol to obtain clean MS spectra free from protein contaminants present in culture media. To achieve this, matched blastomeres and zygote halves were carefully separated, thoroughly washed in pure water, and collected without lysis. While isobaric mass tags enabled multiplexing, they also introduce challenges in reliably quantifying protein abundance in single cells, especially for proteins represented by a single peptide. To strengthen the robustness of our findings, we employed both DDA and DIA, two complementary and orthogonal methods, which yielded consistent results. Future studies could benefit from plexDIA[83] for further mitigation.

We found that protein asymmetry is already established as early as the zygote stage, prior to ZGA, suggesting that symmetry-breaking mechanisms are driven at least in part by post-transcriptional processes. Importantly, we found that parthenogenetic embryos exhibited no proteome asymmetry, and the sperm entry point correlated with the observed gradient of asymmetry—implicating fertilization as a trigger for symmetry breaking. These findings unify decades of observations linking the sperm entry site, blastomere heterogeneity, and cell fate, anchoring them in the landscape of proteomic heterogeneity within early embryos—mapped here using single-cell MS.

The data we present here reveal that proteins involved in protein degradation and transport pathways are not only highly enriched in blastomeres but also differentially enriched between alpha and beta cells. These findings point to a key role for protein turnover and trafficking in initiating cellular divergence prior to overt lineage specification. To demonstrate the functional utility of this resource, we selected three asymmetrically distributed proteins for targeted perturbation in mouse embryos. These experiments revealed effects on lineage contribution, thus establishing a proof-of-principle link between proteomic asymmetry and developmental outcomes. While these three examples serve to illustrate biological relevance, they also highlight the potential for broad, systematic follow-up studies. Future work could explore how these proteins influence fate decisions: is this by modulating lineage-specific differentiation, survival, or proliferation and their molecular interactions and downstream transcriptional effects? In addition, the dataset could serve as a resource for investigating mechanisms regulating the maintenance versus dissolution of totipotency. For example, proteins enriched in beta blastomeres—particularly those involved in protein degradation—may promote more rapid turnover of maternal proteins, impacting ZGA. By contrast, alpha blastomeres, which exhibit higher levels of translation-related proteins, may prolong

(C) A schematic showing the experimental harvesting of zygote halves following labeling of the fertilization cone (FC). Metaphase II stage (MII) oocytes were harvested and fertilized *in vitro* before FC labeling with a fluorescent bead. Zygotes were subsequently bisected meridionally such that one-half had the bead and the other did not.

(D) Representative images of zygotes during FC labeling (left) and following bisection (right).

(E) K-means clustering of FC-labeled zygote halves.

(F) Heatmap of the 201 proteins with significantly differential abundance (p value < 0.05 by Kruskal-Wallis test) between clusters 1 and 2 in FC-labeled zygote halves. n = 12 halves for the FC-labeled zygote stage.

(G) Scatterplot of median protein fold changes between FC-labeled zygote halves on the x axis and median protein fold changes between sister blastomeres at the 2-cell stage. The proteins chosen were both differentially abundant between cluster 1 and cluster 2 at the 2-cell stage and quantified in the FC-labeled zygote halves dataset. We see a significant positive correlation (r = 0.79, p value = 4.27×10^{-14}).

(H) Scatterplot of the median log2 protein fold changes for alpha-beta proteins, which were quantified in both 2-cell-stage sample sets, showing the correlation between independent datasets and suggesting that cluster 1 is alpha-like and cluster 2 is beta-like.

(I) A schematic showing the FC labeling of *in vitro* fertilized MII oocytes, followed by culture to the 2-cell stage, after which sister blastomeres were separated from each other and cultured individually to the late blastocyst stage, and lineage composition was assessed.

(J) Representative examples of "half" blastocysts following FC labeling and splitting at the 2-cell stage, showing the blastocyst descended from the 2-cell-stage blastomere inheriting the FC (with FC) or not (without FC). Images are shown as maximum projections showing the composition of the ICM and the presence or absence of the fluorescent bead (arrowhead). Scale bars, 20 μm.

(K) Boxplots of EPI proportion (Sox17/Cdx2 double-negative cells divided by the total number of DAPI-positive cells in each blastocyst). Blastocysts descended from the blastomere that inherited the FC have a higher EPI proportion. Unpaired t test, p = 0.0298. n = 21 blastocysts with FC and 21 blastocysts without FC.

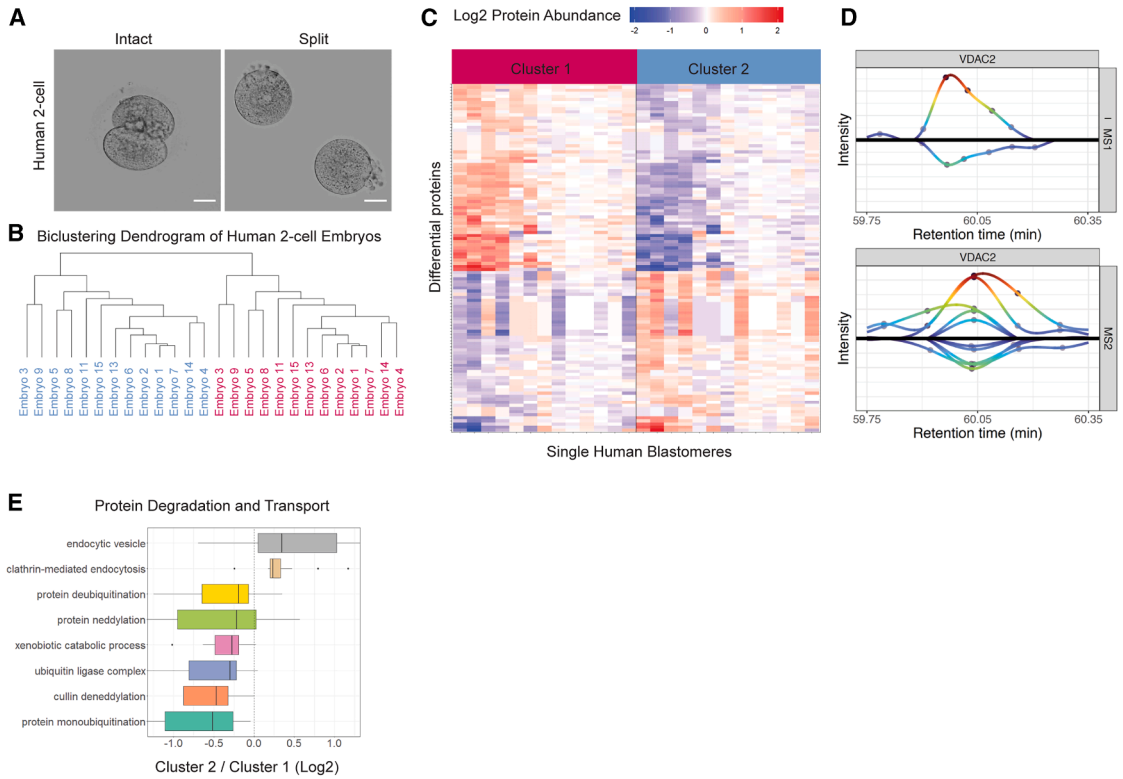

Figure 6. Proteome asymmetry in human 2-cell-stage embryos

(A) Representative images of human 2-cell embryos prior to and following splitting into individual blastomeres. Scale bars, 40 μm.

(B) Dendrogram illustrating the biclustering of human 2-cell-stage blastomeres. Embryo numbers are for indexing purposes only. Color coding indicates the cluster in which each blastomere is classified. n = 13 pairs from human 2-cell embryos.

(C) Heatmap of the 105 proteins that are differentially abundant between the two clusters. Human blastomeres are shown in the same order as the dendrogram on the x axis, while the proteins have been ordered through hierarchical clustering on the y axis.

(D) Extracted ion chromatogram of peptides mapping to VDAC2 on both the MS1 and MS2 levels, indicating consistent fold changes between sister cells.

(E) Boxplots of fold changes between sisters for proteins contributing to protein degradation and protein transport terms, which were found to be significantly differential between clusters in the human 2-cell-stage dataset.

maternal control over development, potentially contributing to their more limited developmental potential.

The proteome asymmetry described here provides a molecular foundation for previous observations of uneven developmental potential and lineage contribution in both mouse[8,10,15,16,51] and human.[9,17–20] Multiple lines of evidence link the division of blastomeres into alpha and beta classes with striking differences in developmental outcomes, despite the highly regulative nature of mammalian development. Our data show that beta blastomeres possess a greater developmental potential than their alpha counterparts, as evidenced by their ability to give rise to blastocysts with more epiblast cells when isolated and cultured independently from each other. Furthermore, vegetal blastomeres at the 4-cell stage, which are known to have reduced developmental potential and have biased to contribute to the TE,[10,51] were more likely to exhibit an alpha proteomic identity than beta identity, linking early molecular asymmetry to downstream cell fate outcomes. Importantly, a similar proteomic dichotomy is observed between the blastomeres of human 2-cell embryos, indicating that early proteomic asymmetry may be a conserved feature of mammalian development.

Throughout our dataset, we observed variability in the extent of alpha-beta polarization, likely reflecting natural differences in cleavage orientation in relation to zygote asymmetry during early divisions. Previous studies have shown that cleavage patterns can influence the cell fate of mouse embryos.[10,11,51] This variability also aligns with earlier findings that, while only one blastomere can give rise to a mouse when isolated from its sister in the majority of 2-cell mouse embryos, in a minority of embryos both sister cells retain such totipotency.[8,16] Together, the findings we present here suggest that early proteome asymmetry underpins symmetry breaking and contributes to variability in developmental potential from the very first divisions of an embryo.

While we did not observe simple 1:1 concordance between mouse and human proteomic profiles, our data point to conserved principles of asymmetric protein inheritance. The enrichment of proteins involved in protein degradation and other post-translational regulatory pathways may reflect a conserved mechanism for early symmetry breaking, with implications for broader developmental biology. Supporting this, a recent study revealed asymmetric lineage contribution in human embryos,[9] reinforcing the cross-species relevance of our findings.

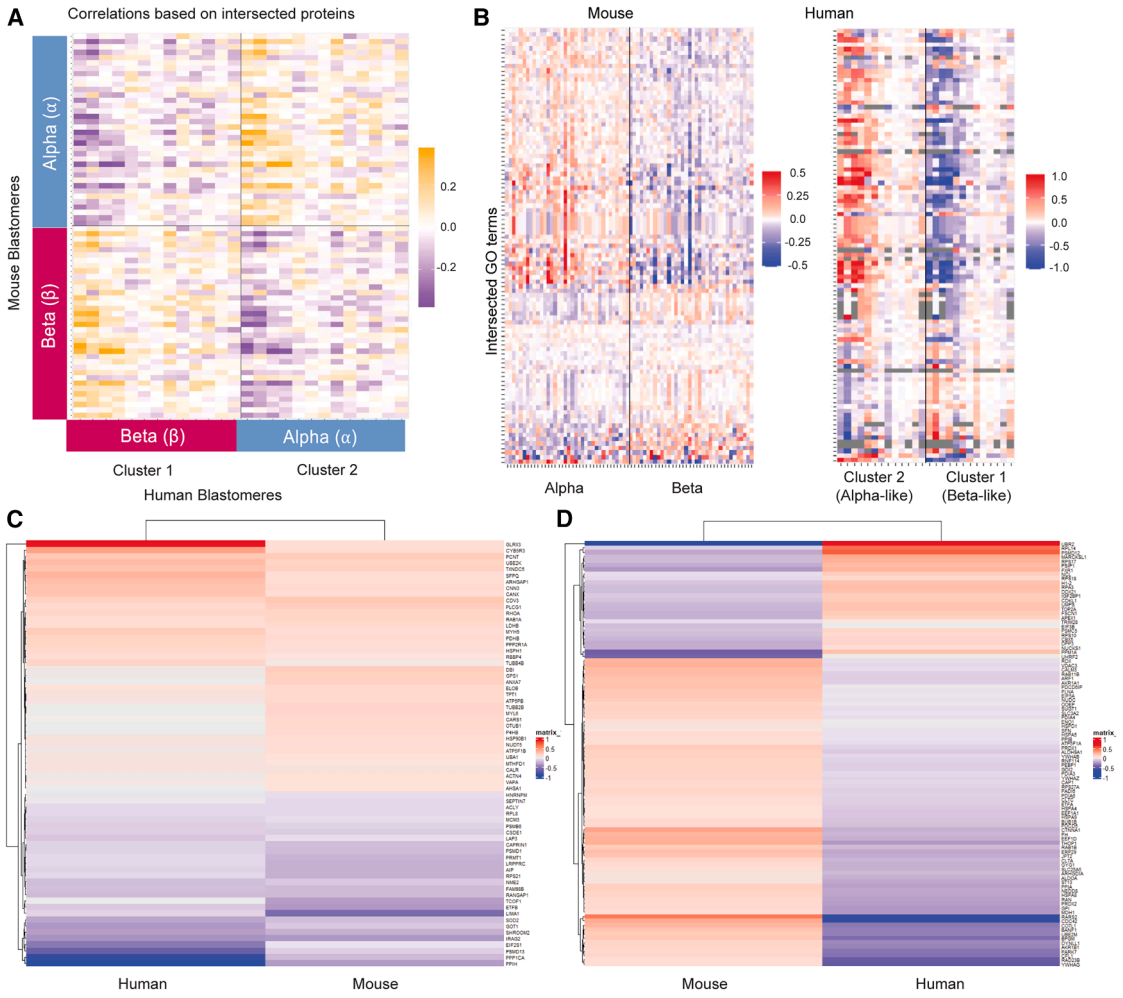

Figure 7. Alpha and beta clusters are conserved in human embryos at the 2-cell stage

(A) Heatmap of pairwise correlations between mouse and human 2-cell-stage blastomeres based on all intersected proteins showing two clusters, and hence, the alignment of alpha and beta classification in mouse with the two human clusters.

(B) Heatmap of the *Z* scores of the median protein abundance for each human blastomere for intersected GO terms that were significantly differential between clusters in mouse and human.

(C and D) Heatmaps of the median fold changes between alpha and beta blastomeres in both mouse and human for proteins that were found to be significantly differential between alpha and beta clusters in mouse embryos. The first heatmap corresponds to proteins that are changing in the same direction across the human and mouse blastomeres. The second heatmap illustrates proteins that have opposing median levels between human and mouse blastomeres.

The results we present here may also help explain the biological underpinnings of diamniotic-dichorionic monozygotic twinning, which likely arises from embryo splitting at various pre-implantation stages and accounts for approximately one-third of monozygotic twin pregnancies.[84] The variable degrees of proteome asymmetry and developmental potential observed[8,9,16] could contribute to this infrequent but biologically significant phenomenon, underscoring the broader relevance of early proteomic asymmetry in mammalian development.

The mechanisms driving asymmetric protein localization remain unclear. Intriguingly, we find that components of cytoplasmic lattices—implicated in maternal protein storage in the oocyte[85]—are unevenly distributed between alpha and beta blastomeres. Two such lattice-associated proteins (Padi6 and Ooep) are enriched in beta cells, and several other lattice-enriched proteins show similar asymmetry. For example, RPs are more abundant in alpha cells, whereas mitochondrial proteins, peroxidase-related proteins, tubulin, and 14-3-3 proteins are enriched in beta cells. These findings suggest that maternally inherited proteins may bias early cell fate decisions as early as the 2-cell stage. Such asymmetry may lead to or be further amplified by asynchronous ZGA, reinforcing transcriptional and proteomic divergence between sister cells as development proceeds to the 4-cell stage.

In summary, our single-cell proteomics approach and functional studies in relation to zygote fertilization uncover the earliest known proteomic asymmetries in the mammalian embryo and identify fertilization as their trigger. These asymmetries align with differences in developmental potential, offering insights into the molecular origins of early heterogeneity and

cell fate bias in the mammalian embryo. By defining alpha and beta proteomic profiles, this work lays the foundation for investigating how early molecular differences influence totipotency and lineage allocation. Clinically, understanding these asymmetries could help optimize assisted reproductive technologies by guiding embryo selection for greater developmental viability.

Limitations of the study

A challenge in this study was validating the proteomic differences identified and quantified by MS using non-MS-based methods. We attempted to use an immunofluorescence-based approach to visualize our data and stained 2-cell-stage mouse embryos for beta-associated proteins (Dppa5a, Cdc42, and Ube2m) and alpha-associated proteins (Ncl, Nedd4l, and Sap18). At the level of individual proteins, significant differences in abundance were detectable (Figures S7A and S7B). However, when multiple proteins were considered collectively, the resulting fold changes did not allow for classification of the blastomeres (Figure S7C). Although both MS and immunofluorescence can theoretically detect low-abundance proteins, there are significant differences. MS quantifies peptides with high specificity, which is very challenging to achieve with antibodies and other affinity reagents. Furthermore, MS often quantifies multiple different peptides per protein, while immunofluorescence relies on individual epitopes, which may be inaccessible. These challenges of epitope specificity and availability, combined with potential variability in staining efficiency across embryos, limited the quantitative reliability of our immunofluorescence analysis. To circumvent this problem, we used two orthogonal MS methods within our manuscript to validate our findings: DDA[40,41] and DIA,[86] which use different ions (precursor ions for DIA and reporter ions for DDA) used for quantitation and thus have minimal shared biases.[81,82]

RESOURCE AVAILABILITY

Lead contact

For additional information or to request resources and reagents, please contact Prof. Magdalena Zernicka-Goetz (magdaz@caltech.edu).

Materials availability

This study did not produce any new, unique reagents. Specific reagents (e.g., plasmids) are available upon request by contacting the lead author.

Data and code availability

- All Metadata, raw data, and processed data are organized according to community recommendations[81] and are available via MassIVE with the dataset identifiers MSV000089353 (ftp://msv000089353@massive.ucsd.edu) and MSV000098778 (ftp://msv000098778@massive-ftp.ucsd.edu).
- All original code has been deposited at Zenodo at https://doi.org/10.5281/zenodo.17469687 and is publicly available as of the date of publication.
- Any additional information required to reanalyze the data reported in this paper is available from the lead contact upon request.

ACKNOWLEDGMENTS

This work is dedicated to the memory of Sir John Gurdon, an extraordinary scientist and mentor, whose vision and curiosity inspired this work and continue to inspire the scientific community. We are thankful to the CARE Fertility Group, Herts & Essex fertility clinics, and USC Fertility for their support. L.K.I.-S. was funded by the Rosetrees Trust (M877). M.M. was supported by the Leverhulme Trust (RPG-2018-085). This work was funded by the Wellcome Trust (207415/Z/17/Z), the Open Philanthropy Grant, the Distinguished Scientist Nomis Award (human embryo work), and the R01HD100456 and R01HD101489 grants from the NIH (mouse embryo and stem cell work) to M.Z.-G. and by a New Innovator award (DP2GM123497) from the NIGMS, R01GM144967 from the NIH, and an Allen Distinguished Investigator award through the Paul G. Allen Frontiers Group to N.S. T.-F.C. and the Proteome Exploration Laboratory were supported by the Caltech Beckman Institute Endowment Funds.

AUTHOR CONTRIBUTIONS

L.K.I.-S. performed human and mouse embryo collection, experimental work, mouse and human stem cell work, and data analysis. M.M., S.N., A.F., B.M., and S.J. helped with mouse embryo experiments and data collection. A.A.P. and B.Q. performed MS sample preparation, maintenance, and data analysis. A.A.P. and N.S. designed data analysis approaches. H.S., G.H., J.D., S.K., and T-Y.W. helped with data analysis and MS maintenance. A.W., B.A.T.W., and C.W.G. performed the human embryo work at Cambridge. L.L., R.S.M., and R.J.P. performed human embryo work in California. L.K.I.-S., N.S., A.A.P., B.Q., and M.Z.-G. wrote the manuscript. L.K.I.-S. and M.Z.-G. conceived the project. T.-F.C., N.S., and M.Z.-G. supervised this work.

DECLARATION OF INTERESTS

The authors have submitted a patent application. N.S. is a founding director and CEO of Parallel Squared Technology Institute, which is a nonprofit research institute.

STAR★METHODS

Detailed methods are provided in the online version of this paper and include the following:

- KEY RESOURCES TABLE
- EXPERIMENTAL MODEL AND STUDY PARTICIPANT DETAILS
  - Mouse embryo culture and sample collection
  - Human Embryo Ethics statement
  - Human embryo culture and sample collection
  - Human stem cell culture and sample collection
- METHOD DETAILS
  - Single-cell sample collection
  - *In vitro* fertilization (IVF) and fertilization cone labelling
  - Parthenogenetic activation of oocytes
  - dsRNA and mRNA synthesis
  - Microinjection
  - qRT-PCR
  - Immunofluorescence and confocal imaging
  - Live Imaging
  - Mouse stem cell culture and sample collection
  - Mass spectrometry (MS) sample preparation
  - Mass spectrometry acquisition methods
  - Analysis of raw SCoPE2 and pSCoPE MS Data
  - Label-free DIA analysis and DIA-NN search parameters
- QUANTIFICATION AND STATISTICAL ANALYSIS
  - Image analysis and statistics
  - K-means Clustering
  - Determining differential proteins between alpha- and beta-cell types
  - Comparison between bulk stem cells and mouse blastomeres
  - Protein Set Enrichment Analysis (PSEA) for Alpha vs Beta Comparison
  - Ribosomal Protein Analysis
  - Vegetal cell analysis
  - Across the stages Analysis
  - Comparison between human and mouse 2-cell embryos

- Cut zygotes analysis
- Split Blastomere Experiment Analysis

SUPPLEMENTAL INFORMATION

Supplemental information can be found online at https://doi.org/10.1016/j.cell.2025.11.006.

Received: October 10, 2024
Revised: April 17, 2025
Accepted: November 5, 2025
Published: December 3, 2025

REFERENCES

1. Niakan, K.K., Han, J., Pedersen, R.A., Simon, C., and Pera, R.A.R. (2012). Human pre-implantation embryo development. Development *139*, 829–841. https://doi.org/10.1242/dev.060426.
2. Zhu, M., and Zernicka-Goetz, M. (2020). Principles of Self-Organization of the Mammalian Embryo. Cell *183*, 1467–1478. https://doi.org/10.1016/j.cell.2020.11.003.
3. Anani, S., Bhat, S., Honma-Yamanaka, N., Krawchuk, D., and Yamanaka, Y. (2014). Initiation of Hippo signaling is linked to polarity rather than to cell position in the pre-implantation mouse embryo. Development *141*, 2813–2824. https://doi.org/10.1242/dev.107276.
4. Morris, S.A., Teo, R.T.Y., Li, H., Robson, P., Glover, D.M., and Zernicka-Goetz, M. (2010). Origin and formation of the first two distinct cell types of the inner cell mass in the mouse embryo. Proc. Natl. Acad. Sci. USA *107*, 6364–6369. https://doi.org/10.1073/pnas.0915063107.
5. Solter, D. (2016). Preformation Versus Epigenesis in Early Mammalian Development. Curr. Top. Dev. Biol. *117*, 377–391. https://doi.org/10.1016/bs.ctdb.2015.11.006.
6. Motosugi, N., Bauer, T., Polanski, Z., Solter, D., and Hiiragi, T. (2005). Polarity of the mouse embryo is established at blastocyst and is not prepatterned. Genes Dev. *19*, 1081–1092. https://doi.org/10.1101/gad.1304805.
7. Dietrich, J.-E., and Hiiragi, T. (2007). Stochastic patterning in the mouse pre-implantation embryo. Development *134*, 4219–4231. https://doi.org/10.1242/dev.003798.
8. Casser, E., Israel, S., Witten, A., Schulte, K., Schlatt, S., Nordhoff, V., and Boiani, M. (2017). Totipotency segregates between the sister blastomeres of two-cell stage mouse embryos. Sci. Rep. *7*, 8299. https://doi.org/10.1038/s41598-017-08266-6.
9. Junyent, S., Meglicki, M., Vetter, R., Mandelbaum, R., King, C., Patel, E.M., Iwamoto-Stohl, L., Reynell, C., Chen, D.-Y., Rubino, P., et al. (2024). The first two blastomeres contribute unequally to the human embryo. Cell *187*, 2838–2854.e17. https://doi.org/10.1016/j.cell.2024.04.029.
10. Piotrowska-Nitsche, K., Perea-Gomez, A., Haraguchi, S., and Zernicka-Goetz, M. (2005). Four-cell stage mouse blastomeres have different developmental properties. Development *132*, 479–490. https://doi.org/10.1242/dev.01602.
11. Torres-Padilla, M.-E., Parfitt, D.-E., Kouzarides, T., and Zernicka-Goetz, M. (2007). Histone arginine methylation regulates pluripotency in the early mouse embryo. Nature *445*, 214–218. https://doi.org/10.1038/nature05458.
12. Goolam, M., Scialdone, A., Graham, S.J.L., Macaulay, I.C., Jedrusik, A., Hupalowska, A., Voet, T., Marioni, J.C., and Zernicka-Goetz, M. (2016). Heterogeneity in Oct4 and Sox2 Targets Biases Cell Fate in 4-Cell Mouse Embryos. Cell *165*, 61–74. https://doi.org/10.1016/j.cell.2016.01.047.
13. Chen, Q., Shi, J., Tao, Y., and Zernicka-Goetz, M. (2018). Tracing the origin of heterogeneity and symmetry breaking in the early mammalian embryo. Nat. Commun. *9*, 1819. https://doi.org/10.1038/s41467-018-04155-2.
14. Gardner, R.L. (2001). Specification of embryonic axes begins before cleavage in normal mouse development. Development *128*, 839–847. https://doi.org/10.1242/dev.128.6.839.
15. Piotrowska, K., and Zernicka-Goetz, M. (2002). Early patterning of the mouse embryo–contributions of sperm and egg. Development *129*, 5803–5813. https://doi.org/10.1242/dev.00170.
16. Tsunoda, Y., and McLaren, A. (1983). Effect of various procedures on the viability of mouse embryos containing half the normal number of blastomeres. J. Reprod. Fertil. *69*, 315–322. https://doi.org/10.1530/jrf.0.0690315.
17. Coorens, T.H.H., Moore, L., Robinson, P.S., Sanghvi, R., Christopher, J., Hewinson, J., Przybilla, M.J., Lawson, A.R.J., Chapman, M.S., Cagan, A., et al. (2021). Extensive phylogenies of human development inferred from somatic mutations. Nature *597*, 387–392. https://doi.org/10.1038/s41586-021-03790-y.
18. Coorens, T.H.H., Oliver, T.R.W., Sanghvi, R., Sovio, U., Cook, E., Vento-Tormo, R., Haniffa, M., Young, M.D., Rahbari, R., Sebire, N., et al. (2021). Inherent mosaicism and extensive mutation of human placentas. Nature *592*, 80–85. https://doi.org/10.1038/s41586-021-03345-1.
19. Fasching, L., Jang, Y., Tomasi, S., Schreiner, J., Tomasini, L., Brady, M.V., Bae, T., Sarangi, V., Vasmatzis, N., Wang, Y., et al. (2021). Early developmental asymmetries in cell lineage trees in living individuals. Science *371*, 1245–1248. https://doi.org/10.1126/science.abe0981.
20. Spencer Chapman, M.S., Ranzoni, A.M., Myers, B., Williams, N., Coorens, T.H.H., Mitchell, E., Butler, T., Dawson, K.J., Hooks, Y., Moore, L., et al. (2021). Lineage tracing of human development through somatic mutations. Nature *595*, 85–90. https://doi.org/10.1038/s41586-021-03548-6.
21. Bizzotto, S., Dou, Y., Ganz, J., Doan, R.N., Kwon, M., Bohrson, C.L., Kim, S.N., Bae, T., and Abyzov, A.; NIMH; Brain; Somatic; Mosaicism Network (2021). Landmarks of human embryonic development inscribed in somatic mutations. Science *371*, 1249–1253. https://doi.org/10.1126/science.abe1544.
22. Kim-Ha, J., Smith, J.L., and Macdonald, P.M. (1991). oskar mRNA is localized to the posterior pole of the Drosophila oocyte. Cell *66*, 23–35. https://doi.org/10.1016/0092-8674(91)90136-M.
23. Driever, W., and Nüsslein-Volhard, C. (1988). A gradient of bicoid protein in Drosophila embryos. Cell *54*, 83–93. https://doi.org/10.1016/0092-8674(88)90182-1.
24. St Johnston, D., Driever, W., Berleth, T., Richstein, S., and Nüsslein-Volhard, C. (1989). Multiple steps in the localization of bicoid RNA to the anterior pole of the Drosophila oocyte. Development *107*, 13–19. https://doi.org/10.1242/dev.107.Supplement.13.
25. Wang, C., and Lehmann, R. (1991). Nanos is the localized posterior determinant in Drosophila. Cell *66*, 637–647. https://doi.org/10.1016/0092-8674(91)90110-k.
26. Roberts, R.M., Katayama, M., Magnuson, S.R., Falduto, M.T., and Torres, K.E.O. (2011). Transcript profiling of individual twin blastomeres derived by splitting two-cell stage murine embryos. Biol. Reprod. *84*, 487–494. https://doi.org/10.1095/biolreprod.110.086884.
27. Tang, F., Barbacioru, C., Nordman, E., Bao, S., Lee, C., Wang, X., Tuch, B.B., Heard, E., Lao, K., and Surani, M.A. (2011). Deterministic and Stochastic Allele Specific Gene Expression in Single Mouse Blastomeres. PLoS One *6*, e21208. https://doi.org/10.1371/journal.pone.0021208.
28. Biase, F.H., Cao, X., and Zhong, S. (2014). Cell fate inclination within 2-cell and 4-cell mouse embryos revealed by single-cell RNA sequencing. Genome Res. *24*, 1787–1796. https://doi.org/10.1101/gr.177725.114.
29. Wang, J., Wang, L., Feng, G., Wang, Y., Li, Y., Li, X., Liu, C., Jiao, G., Huang, C., Shi, J., et al. (2018). Asymmetric Expression of LincGET Biases Cell Fate in Two-Cell Mouse Embryos. Cell *175*, 1887–1901.e18. https://doi.org/10.1016/j.cell.2018.11.039.
30. Casser, E., Israel, S., Schlatt, S., Nordhoff, V., and Boiani, M. (2018). Retrospective analysis: reproducibility of interblastomere differences of mRNA expression in 2-cell stage mouse embryos is remarkably poor due to combinatorial mechanisms of blastomere diversification. Mol. Hum. Reprod. *24*, 388–400. https://doi.org/10.1093/molehr/gay021.

31. Franks, A., Airoldi, E., and Slavov, N. (2017). Post-transcriptional regulation across human tissues. PLoS Comput. Biol. *13*, e1005535. https://doi.org/10.1371/journal.pcbi.1005535.

32. Nothias, J.Y., Miranda, M., and DePamphilis, M.L. (1996). Uncoupling of transcription and translation during zygotic gene activation in the mouse. EMBO J. *15*, 5715–5725. https://doi.org/10.1002/j.1460-2075.1996.tb00955.x.

33. Lombard-Banek, C., Li, J., Portero, E.P., Onjiko, R.M., Singer, C.D., Plotnick, D.O., Al Shabeeb, R.Q., and Nemes, P. (2021). In Vivo Subcellular Mass Spectrometry Enables Proteo-Metabolomic Single-Cell Systems Biology in a Chordate Embryo Developing to a Normally Behaving Tadpole (X. laevis)*. Angew. Chem. Int. Ed. Engl. *60*, 12852–12858. https://doi.org/10.1002/anie.202100923.

34. Lombard-Banek, C., Moody, S.A., and Nemes, P. (2016). Single-cell mass spectrometry for discovery proteomics: Quantifying translational cell heterogeneity in the 16-cell frog (Xenopus) embryo. Angew. Chem. *128*, 2500–2504. https://doi.org/10.1002/ange.201510411.

35. Virant-Klun, I., Leicht, S., Hughes, C., and Krijgsveld, J. (2016). Identification of Maturation-Specific Proteins by Single-Cell Proteomics of Human Oocytes. Mol. Cell. Proteomics *15*, 2616–2627. https://doi.org/10.1074/mcp.M115.056887.

36. Wang, S., Kou, Z., Jing, Z., Zhang, Y., Guo, X., Dong, M., Wilmut, I., and Gao, S. (2010). Proteome of mouse oocytes at different developmental stages. Proc. Natl. Acad. Sci. USA *107*, 17639–17644. https://doi.org/10.1073/pnas.1013185107.

37. Gao, Y., Liu, X., Tang, B., Li, C., Kou, Z., Li, L., Liu, W., Wu, Y., Kou, X., Li, J., et al. (2017). Protein Expression Landscape of Mouse Embryos during Pre-implantation Development. Cell Rep. *21*, 3957–3969. https://doi.org/10.1016/j.celrep.2017.11.111.

38. Israel, S., Ernst, M., Psathaki, O.E., Drexler, H.C.A., Casser, E., Suzuki, Y., Makalowski, W., Boiani, M., Fuellen, G., and Taher, L. (2019). An integrated genome-wide multi-omics analysis of gene expression dynamics in the preimplantation mouse embryo. Sci. Rep. *9*, 13356. https://doi.org/10.1038/s41598-019-49817-3.

39. Hamatani, T., Carter, M.G., Sharov, A.A., and Ko M, S. (2004). Dynamics of global gene expression changes during mouse preimplantation development. Dev. Cell *6*, 117–131. https://doi.org/10.1016/s1534-5807(03)00373-3.

40. Petelski, A.A., Emmott, E., Leduc, A., Huffman, R.G., Specht, H., Perlman, D.H., and Slavov, N. (2021). Multiplexed single-cell proteomics using SCoPE2. Nat. Protoc. *16*, 5398–5425. https://doi.org/10.1038/s41596-021-00616-z.

41. Specht, H., Emmott, E., Petelski, A.A., Huffman, R.G., Perlman, D.H., Serra, M., Kharchenko, P., Koller, A., and Slavov, N. (2021). Single-cell proteomic and transcriptomic analysis of macrophage heterogeneity using SCoPE2. Genome Biol. *22*, 50. https://doi.org/10.1186/s13059-021-02267-5.

42. Budnik, B., Levy, E., Harmange, G., and Slavov, N. (2018). SCoPE-MS: mass spectrometry of single mammalian cells quantifies proteome heterogeneity during cell differentiation. Genome Biol. *19*, 161. https://doi.org/10.1186/s13059-018-1547-5.

43. Yurttas, P., Vitale, A.M., Fitzhenry, R.J., Cohen-Gould, L., Wu, W., Gossen, J.A., and Coonrod, S.A. (2008). Role for PADI6 and the cytoplasmic lattices in ribosomal storage in oocytes and translational control in the early mouse embryo. Development *135*, 2627–2636. https://doi.org/10.1242/dev.016329.

44. Esposito, G., Vitale, A.M., Leijten, F.P.J., Strik, A.M., Koonen-Reemst, A.M.C.B., Yurttas, P., Robben, T.J.A.A., Coonrod, S., and Gossen, J.A. (2007). Peptidylarginine deiminase (PAD) 6 is essential for oocyte cytoskeletal sheet formation and female fertility. Mol. Cell. Endocrinol. *273*, 25–31. https://doi.org/10.1016/j.mce.2007.05.005.

45. Liu, M., Oh, A., Calarco, P., Yamada, M., Coonrod, S.A., and Talbot, P. (2005). Peptidylarginine deiminase (PAD) is a mouse cortical granule protein that plays a role in preimplantation embryonic development. Reprod. Biol. Endocrinol. *3*, 42. https://doi.org/10.1186/1477-7827-3-42.

46. Zhou, S., Guo, Y., Sun, H., Liu, L., Yao, L., Liu, C., He, Y., Cao, S., Zhou, C., Li, M., et al. (2021). Maternal RNF114-mediated target substrate degradation regulates zygotic genome activation in mouse embryos. Development *148*, dev199426. https://doi.org/10.1242/dev.199426.

47. Yang, Y., Zhou, C., Wang, Y., Liu, W., Liu, C., Wang, L., Liu, Y., Shang, Y., Li, M., Zhou, S., et al. (2017). The E3 ubiquitin ligase RNF114 and TAB1 degradation are required for maternal-to-zygotic transition. EMBO Rep. *18*, 205–216. https://doi.org/10.15252/embr.201642573.

48. Matsumoto, H., Daikoku, T., Wang, H., Sato, E., and Dey, S.K. (2004). Differential expression of ezrin/radixin/moesin (ERM) and ERM-associated adhesion molecules in the blastocyst and uterus suggests their functions during implantation. Biol. Reprod. *70*, 729–736. https://doi.org/10.1095/biolreprod.103.022764.

49. Cui, X.-S., Li, X.-Y., and Kim, N.-H. (2007). Cdc42 is implicated in polarity during meiotic resumption and blastocyst formation in the mouse. Mol. Reprod. Dev. *74*, 785–794. https://doi.org/10.1002/mrd.20571.

50. Korotkevich, E., Niwayama, R., Courtois, A., Friese, S., Berger, N., Buchholz, F., and Hiiragi, T. (2017). The Apical Domain Is Required and Sufficient for the First Lineage Segregation in the Mouse Embryo. Dev. Cell *40*, 235–247.e7. https://doi.org/10.1016/j.devcel.2017.01.006.

51. Morris, S.A., Guo, Y., and Zernicka-Goetz, M. (2012). Developmental plasticity is bound by pluripotency and the Fgf and Wnt signaling pathways. Cell Rep. *2*, 756–765. https://doi.org/10.1016/j.celrep.2012.08.029.

52. White, M.D., Angiolini, J.F., Alvarez, Y.D., Kaur, G., Zhao, Z.W., Mocskos, E., Bruno, L., Bissiere, S., Levi, V., and Plachta, N. (2016). Long-Lived Binding of Sox2 to DNA Predicts Cell Fate in the Four-Cell Mouse Embryo. Cell *165*, 75–87. https://doi.org/10.1016/j.cell.2016.02.032.

53. Hupalowska, A., Jedrusik, A., Zhu, M., Bedford, M.T., Glover, D.M., and Zernicka-Goetz, M. (2018). CARM1 and Paraspeckles Regulate Preimplantation Mouse Embryo Development. Cell *175*, 1902–1916.e13. https://doi.org/10.1016/j.cell.2018.11.027.

54. Burton, A., Muller, J., Tu, S., Padilla-Longoria, P., Guccione, E., and Torres-Padilla, M.-E. (2013). Single-Cell Profiling of Epigenetic Modifiers Identifies PRDM14 as an Inducer of Cell Fate in the Mammalian Embryo. Cell Rep. *5*, 687–701. https://doi.org/10.1016/j.celrep.2013.09.044.

55. Gardner, R.L. (2002). Experimental analysis of second cleavage in the mouse. Hum. Reprod. *17*, 3178–3189. https://doi.org/10.1093/humrep/17.12.3178.

56. Gardner, R.L. (1997). The early blastocyst is bilaterally symmetrical and its axis of symmetry is aligned with the animal-vegetal axis of the zygote in the mouse. Development *124*, 289–301. https://doi.org/10.1242/dev.124.2.289.

57. Plusa, B., Grabarek, J.B., Piotrowska, K., Glover, D.M., and Zernicka-Goetz, M. (2002). Site of the previous meiotic division defines cleavage orientation in the mouse embryo. Nat. Cell Biol. *4*, 811–815. https://doi.org/10.1038/ncb860.

58. Li, L., Baibakov, B., and Dean, J. (2008). A subcortical maternal complex essential for preimplantation mouse embryogenesis. Dev. Cell *15*, 416–425. https://doi.org/10.1016/j.devcel.2008.07.010.

59. Shin, S.-W., Tokoro, M., Nishikawa, S., Lee, H.-H., Hatanaka, Y., Nishihara, T., Amano, T., Anzai, M., Kato, H., Mitani, T., et al. (2010). Inhibition of the Ubiquitin-proteasome System Leads to Delay of the Onset of ZGA Gene Expression. J. Reprod. Dev. *56*, 655–663. https://doi.org/10.1262/jrd.10-104m.

60. Shin, S.-W., Shimizu, N., Tokoro, M., Nishikawa, S., Hatanaka, Y., Anzai, M., Hamazaki, J., Kishigami, S., Saeki, K., Hosoi, Y., et al. (2013). Mouse zygote-specific proteasome assembly chaperone important for maternal-to-zygotic transition. Biol. Open *2*, 170–182. https://doi.org/10.1242/bio.20123020.

61. Higuchi, C., Shimizu, N., Shin, S.-W., Morita, K., Nagai, K., Anzai, M., Kato, H., Mitani, T., Yamagata, K., Hosoi, Y., et al. (2018). Ubiquitin-proteasome system modulates zygotic genome activation in early mouse embryos and

influences full-term development. J. Reprod. Dev. *64*, 65–74. https://doi.org/10.1262/jrd.2017-127.

62. Kondrashov, N., Pusic, A., Stumpf, C.R., Shimizu, K., Hsieh, A.C., Ishijima, J., Shiroishi, T., and Barna, M. (2011). Ribosome-Mediated Specificity in Hox mRNA Translation and Vertebrate Tissue Patterning. Cell *145*, 383–397. https://doi.org/10.1016/j.cell.2011.03.028.
63. Norris, K., Hopes, T., and Aspden, J.L. (2021). Ribosome heterogeneity and specialization in development. Wiley Interdiscip. Rev., RNA *12*, e1644. https://doi.org/10.1002/wrna.1644.
64. Slavov, N., Semrau, S., Airoldi, E., Budnik, B., and van van Oudenaarden, A. (2015). Differential Stoichiometry among Core Ribosomal Proteins. Cell Rep. *13*, 865–873. https://doi.org/10.1016/j.celrep.2015.09.056.
65. Shi, Z., Fujii, K., Kovary, K.M., Genuth, N.R., Röst, H.L., Teruel, M.N., and Barna, M. (2017). Heterogeneous Ribosomes Preferentially Translate Distinct Subpools of mRNAs Genome-wide. Mol. Cell *67*, 71–83.e7. https://doi.org/10.1016/j.molcel.2017.05.021.
66. Tateishi, K., Omata, M., Tanaka, K., and Chiba, T. (2001). The NEDD8 system is essential for cell cycle progression and morphogenetic pathway in mice. J. Cell Biol. *155*, 571–579. https://doi.org/10.1083/jcb.200104035.
67. Wei, N., and Deng, X.W. (2003). The COP9 signalosome. Annu. Rev. Cell Dev. Biol. *19*, 261–286. https://doi.org/10.1146/annurev.cellbio.19.111301.112449.
68. Israel, S., Drexler, H.C.A., Fuellen, G., and Boiani, M. (2021). The COP9 signalosome subunit 3 is necessary for early embryo survival by way of a stable protein deposit in mouse oocytes. Mol. Hum. Reprod. *27*, gaab048. https://doi.org/10.1093/molehr/gaab048.
69. Zhang, W., Ni, P., Mou, C., Zhang, Y., Guo, H., Zhao, T., Loh, Y.-H., and Chen, L. (2016). Cops2 promotes pluripotency maintenance by Stabilizing Nanog Protein and Repressing Transcription. Sci. Rep. *6*, 26804. https://doi.org/10.1038/srep26804.
70. Yan, J., Walz, K., Nakamura, H., Carattini-Rivera, S., Zhao, Q., Vogel, H., Wei, N., Justice, M.J., Bradley, A., and Lupski, J.R. (2003). COP9 Signalosome Subunit 3 Is Essential for Maintenance of Cell Proliferation in the Mouse Embryonic Epiblast. Mol. Cell. Biol. *23*, 6798–6808. https://doi.org/10.1128/mcb.23.19.6798-6808.2003.
71. Chia, N.-Y., Chan, Y.-S., Feng, B., Lu, X., Orlov, Y.L., Moreau, D., Kumar, P., Yang, L., Jiang, J., Lau, M.-S., et al. (2010). A genome-wide RNAi screen reveals determinants of human embryonic stem cell identity. Nature *468*, 316–320. https://doi.org/10.1038/nature09531.
72. Sakao, Y., Kawai, T., Takeuchi, O., Copeland, N.G., Gilbert, D.J., Jenkins, N.A., Takeda, K., and Akira, S. (2000). Mouse Proteasomal ATPases Psmc3 and Psmc4: Genomic Organization and Gene Targeting. Genomics *67*, 1–7. https://doi.org/10.1006/geno.2000.6231.
73. Zernicka-Goetz, M., Pines, J., McLean Hunter, S.M., Dixon, J.P.C., Siemering, K.R., Haseloff, J., and Evans, M.J. (1997). Following cell fate in the living mouse embryo. Development *124*, 1133–1137. https://doi.org/10.1242/dev.124.6.1133.
74. Wianny, F., and Zernicka-Goetz, M. (2000). Specific interference with gene function by double-stranded RNA in early mouse development. Nat. Cell Biol. *2*, 70–75. https://doi.org/10.1038/35000016.
75. Krawczyk, K., Kosyl, E., Częścik-Łysyszyn, K., Wyszomirski, T., and Maleszewski, M. (2021). Developmental capacity is unevenly distributed among single blastomeres of 2-cell and 4-cell stage mouse embryos. Sci. Rep. *11*, 21422. https://doi.org/10.1038/s41598-021-00834-1.
76. Huffman, R.G., Leduc, A., Wichmann, C., Di Gioia, M., Borriello, F., Specht, H., Derks, J., Khan, S., Khoury, L., Emmott, E., et al. (2023). Prioritized mass spectrometry increases the depth, sensitivity and data completeness of single-cell proteomics. Nat. Methods *20*, 714–722. https://doi.org/10.1038/s41592-023-01830-1.
77. Jin, H., Han, Y., Wang, H., Li, J.X.H., Shen, W., Zhang, L., Chen, L., Jia, S., Yuan, P., Chen, H., et al. (2022). The second polar body contributes to the fate asymmetry in the mouse embryo. Natl. Sci. Rev. *9*, nwac003. https://doi.org/10.1093/nsr/nwac003.
78. Strauss, B., Harrison, A., Coelho, P.A., Yata, K., Zernicka-Goetz, M., and Pines, J. (2018). Cyclin B1 is essential for mitosis in mouse embryos, and its nuclear export sets the time for mitosis. J. Cell Biol. *217*, 179–193. https://doi.org/10.1083/jcb.201612147.
79. Leonhardt, H., Rahn, H.P., Weinzierl, P., Sporbert, A., Cremer, T., Zink, D., and Cardoso, M.C. (2000). Dynamics of DNA Replication Factories in Living Cells. J. Cell Biol. *149*, 271–280. https://doi.org/10.1083/jcb.149.2.271.
80. Piotrowska, K., and Zernicka-Goetz, M. (2001). Role for sperm in spatial patterning of the early mouse embryo. Nature *409*, 517–521. https://doi.org/10.1038/35054069.
81. Gatto, L., Aebersold, R., Cox, J., Demichev, V., Derks, J., Emmott, E., Franks, A.M., Ivanov, A.R., Kelly, R.T., Khoury, L., et al. (2023). Initial recommendations for performing, benchmarking and reporting single-cell proteomics experiments. Nat. Methods *20*, 375–386. https://doi.org/10.1038/s41592-023-01785-3.
82. Leduc, A., Huffman, R.G., Cantlon, J., Khan, S., and Slavov, N. (2022). Exploring functional protein covariation across single cells using nPOP. Genome Biol. *23*, 261. https://doi.org/10.1186/s13059-022-02817-5.
83. Derks, J., Leduc, A., Wallmann, G., Huffman, R.G., Willetts, M., Khan, S., Specht, H., Ralser, M., Demichev, V., and Slavov, N. (2023). Increasing the throughput of sensitive proteomics by plexDIA. Nat. Biotechnol. *41*, 50–59. https://doi.org/10.1038/s41587-022-01389-w.
84. Corner, G.W. (1955). The observed embryology of human single-ovum twins and other multiple births. Am. J. Obstet. Gynecol. *70*, 933–951. https://doi.org/10.1016/0002-9378(55)90001-6.
85. Jentoft, I.M.A., Bäuerlein, F.J.B., Welp, L.M., Cooper, B.H., Petrovic, A., So, C., Penir, S.M., Politi, A.Z., Horokhovskyi, Y., Takala, I., et al. (2023). Mammalian oocytes store proteins for the early embryo on cytoplasmic lattices. Cell *186*, 5308–5327.e25. https://doi.org/10.1016/j.cell.2023.10.003.
86. Venable, J.D., Dong, M.-Q., Wohlschlegel, J., Dillin, A., and Yates, J.R. (2004). Automated approach for quantitative analysis of complex peptide mixtures from tandem mass spectra. Nat. Methods *1*, 39–45. https://doi.org/10.1038/nmeth705.
87. Amadei, G., Lau, K.Y.C., De Jonghe, J., Gantner, C.W., Sozen, B., Chan, C., Zhu, M., Kyprianou, C., Hollfelder, F., and Zernicka-Goetz, M. (2021). Inducible Stem-Cell-Derived Embryos Capture Mouse Morphogenetic Events In Vitro. Dev. Cell *56*, 366–382.e9. https://doi.org/10.1016/j.devcel.2020.12.004.
88. Schindelin, J., Arganda-Carreras, I., Frise, E., Kaynig, V., Longair, M., Pietzsch, T., Preibisch, S., Rueden, C., Saalfeld, S., Schmid, B., et al. (2012). Fiji: an open-source platform for biological-image analysis. Nat. Methods *9*, 676–682. https://doi.org/10.1038/nmeth.2019.
89. Lovell-Badge, R., Anthony, E., Barker, R.A., Bubela, T., Brivanlou, A.H., Carpenter, M., Charo, R.A., Clark, A., Clayton, E., Cong, Y., et al. (2021). ISSCR Guidelines for Stem Cell Research and Clinical Translation: The 2021 update. Stem Cell Rep. *16*, 1398–1408. https://doi.org/10.1016/j.stemcr.2021.05.012.
90. Casser, E., Wdowik, S., Israel, S., Witten, A., Schlatt, S., Nordhoff, V., and Boiani, M. (2019). Differences in blastomere totipotency in 2-cell mouse embryos are a maternal trait mediated by asymmetric mRNA distribution. Mol. Hum. Reprod. *25*, 729–744. https://doi.org/10.1093/molehr/gaz051.
91. Horn, T., and Boutros, M. (2010). E-RNAi: a web application for the multi-species design of RNAi reagents—2010 update. Nucleic Acids Res. *38*, W332–W339. https://doi.org/10.1093/nar/gkq317.
92. Chen, A.T., Franks, A., and Slavov, N. (2019). DART-ID increases single-cell proteome coverage. PLoS Comput. Biol. *15*, e1007082. https://doi.org/10.1371/journal.pcbi.1007082.
93. Demichev, V., Messner, C.B., Vernardis, S.I., Lilley, K.S., and Ralser, M. (2020). DIA-NN: neural networks and interference correction enable deep proteome coverage in high throughput. Nat. Methods *17*, 41–44. https://doi.org/10.1038/s41592-019-0638-x.

STAR★METHODS

KEY RESOURCES TABLE

REAGENT or RESOURCE	SOURCE	IDENTIFIER
Antibodies		
Goat anti-Sox17 primary antibody	R&D systems	Cat# AF1924; RRID: AB_355060
Rabbit polyclonal anti-RFP primary antibody	Rockland	Cat# 600-401-379; RRID: AB_2209751
Mouse anti-Cdx2 primary antibody	Launch Diagnostics (Biogenix)	Cat# MU392-UC; RRID:AB_2923402
Rabbit anti-Nanog primary antibody	Abcam	Cat# ab80892; RRID:AB_2150114
Donkey anti-Mouse IgG (H+L) Highly CrossAdsorbed Secondary Antibody, Alexa Fluor 488	Thermo Fisher Scientific	Cat# A-21202; RRID: AB_141607
Donkey anti-Rabbit IgG (H+L) Highly CrossAdsorbed Secondary Antibody, Alexa Fluor 568	Thermo Fisher Scientific	Cat# A10042; RRID: AB_2534017
Donkey anti-Goat IgG (H+L) CrossAdsorbed Secondary Antibody, Alexa Fluor 647	Thermo Fisher Scientific	Cat# A-21447; RRID: AB_2535864
Chemicals, peptides, and recombinant proteins		
M2 medium	Millipore-Sigma	Cat# M7167-100ML
EmbryoMax® Advanced KSOM Medium	Millipore-Sigma	Cat# MR-106-D
Hyaluronidase	Sigma-Aldrich	Cat# H4272
Tyrode's solution	Sigma-Aldrich	Cat# T1788
Optima LC/MS Grade water	Fisher Scientific	Cat# W6500
Global Total culture medium	LifeGlobal group	Cat# H5GT-030
CARD medium	Kyudo	Cat# KYD-005-EX
Phytohaemagglutinin	Sigma-Aldrich	Cat# L8754
$SrCl_2$	Sigma-Aldrich	Cat# 439665
mMessage mMachine T3 kit	Thermo Fisher	Cat# AM1348
MEGAscript T7 kit	Thermo Fisher	Cat# AM1334
Power SYBR Green RNA-to-CT 1-Step Kit	Life Technologies	Cat# 4389986
Arcturus PicoPure RNA isolation kit	Arcturus Bioscience	Cat# KIT0204
Doxycycline	Sigma-Aldrich	Cat# D9891-5G
Origio thaw kit	Origio	Cat# REF10984010A
Embryo Thaw Media Kit	Fujifilm Irvine Scientific	Cat# 90124
Continuous Single Culture-NX Complete medium	Fujifilm Irvine Scientific	Cat# 90168
Deposited data		
Dataset generated at Northeastern University	Generated within this study	massIVE: MSV000089353 (ftp://msv000089353@massive.ucsd.edu)
Code	Generated within this study	Zenodo: https://doi.org/10.5281/zenodo.17469687
Dataset generated at California Institute of Technology	Generated within this study	massIVE: MSV000098778 (ftp://msv000098778@massive-ftp.ucsd.edu)
Experimental models: Cell lines		
Mouse: CAG-GFP/tetO-mCherry ESCs	Amadei et al.[87]	https://doi.org/10.1016/j.devcel.2020.12.004
RUES2 hESCs	Gift from Ali Brivanlou	NA
Experimental models: Organisms/strains		
B6SJLF1/J mice	The Jackson Laboratory	Cat# 100012; RRID: IMSR_JAX:100012

(*Continued on next page*)

Continued		
REAGENT or RESOURCE	SOURCE	IDENTIFIER
Human embryos	HRC Fertility Clinic 55 S. Lake Ave, 9th Fl. Pasadena CA 91101, USA	N/A
Human embryos	CARE Fertility Group and Herts & Essex fertility clinics	N/A
Recombinant DNA		
pRN3P-mCherry	Generated within this study	N/A
pRN3P-Gap43-RFP	Torres-Padilla et al.[11]	https://doi.org/10.1038/nature05458; https://idp.nature.com/authorize?response_type=cookie&client_id=grover&redirect_uri=https%3A%2F%2Fwww.nature.com%2Farticles%2Fnature05458
pRN3P-PCNA-Clover	Gift from Charlotte Handford	N/A
Software and algorithms		
Fiji (ImageJ)	Schindelin et al.[88]	https://fiji.sc/; RRID: SCR_002285
Proteome Discoverer 3.0	Thermo Scientific	CSW0064764
MaxQuant (version 1.6.17)	MaxQuant	RRID:SCR_014485

EXPERIMENTAL MODEL AND STUDY PARTICIPANT DETAILS

Mouse embryo culture and sample collection

This research adhered to the regulations of the Animals (Scientific Procedures) Act 1986 - Amendment Regulations 2012 and was reviewed by the University of Cambridge Animal Welfare and Ethical Review Body. Experiments were approved by the UK Home Office.

Embryos were collected from 4-6 week old F1 females (C57Bl6 x CBA, Charles River) following superovulation by injection of 5 IU of pregnant mares' serum gonadotropin (PMSG, Intervet) and 5 IU of human chorionic gonadotropin (hCG, Intervet) 48 hrs later. Females were mated with F1 males (6 weeks - 52 weeks of age, C57Bl6 x CBA, Charles River). Plugged females were culled by cervical dislocation to recover embryos at the required stage. Embryos, other than zygotes, were recovered in M2 medium (in house).

Zygote stage: zygote stage embryos (22 hrs post-hCG) were recovered in M2 medium with 1mg/ml of hyaluronidase (Sigma, H4272) in order to remove cumulus cells and subsequently washed through M2 medium without hyaluronidase. Samples were collected at 23-24 hrs post-hCG.

Early 2-cell stage: zygote stage embryos (29 hrs post-hCG) were recovered in hyaluronidase as above and subsequently cultured for 1-3h during division from the zygote to 2-cell stage. Following division to the 2-cell stage, samples were collected at 30-32 hrs post-hCG.

Late 2-cell stage: 2-cell stage embryos were recovered at 45 hrs post-hCG and samples collected at 46-48 hrs post-hCG.

4-cell stage: mid to late 2-cell stage embryos were recovered and one sister blastomere was microinjected as described below, to allow for identification of the 4-cell stage sisters originating from the injected 2-cell stage blastomere (mCherry positive pairs were distinguished by SCoPE2). The embryos were transferred to KSOM (Merck, MR-106-D), and live imaged during division from the 2- to 4-cell stage and collected at 55-57 hrs post-hCG. Division pattern, age post-division (2- to 4-cell stage) and division order were annotated for each embryo prior to collection. Uninjected and unimaged controls were also collected with the same timings.

Human Embryo Ethics statement

Human embryo samples for this study were collected in two different institutes: the University of Cambridge (United Kingdom), and the California Institute of Technology (United States). All the work complies with The International Society for Stem Cell Research (ISSCR) guidelines,[89] The work performed here with human embryos is subject to recommendations based on Category 2a (Section 2.2.2a Procurement and use of IVF human embryos for research in vitro) under the ISSCR guidelines, and is thereby permissible after ethical review and approval by relevant oversight bodies.

Human embryo work at the University of Cambridge was performed in accordance with Human Fertility and Embryology Authority (HFEA) regulations (license reference R0193). Ethical approval for the work was obtained from the 'Human Biology Research Ethics Committee' at the University of Cambridge (reference HBREC.2021.26) for the project 'Investigating human development: from pre-implantation to gastrulation'. Informed consent was obtained from all participants in the study which included patients from the CARE Fertility Group and Herts & Essex fertility clinics. Supernumerary embryos were donated upon completion of IVF treatment. Patients

were informed about the specific objectives of the project, and the conditions that apply within the license, before giving consent. Patients were also offered counselling and did not receive any financial inducements for their donation.

Human embryo work at the California Institute of Technology was approved by the California Institute of Technology Committee for the Protection of Human Subjects (IRB number 19–0948: 'A dynamic, multi-dimensional atlas of the human embryo: Guiding the discovery of new pathways of development'). Human embryos at the two pronuclei stage were obtained from the University of Southern California (USC) through the pre-existing USC IRB-approved Biospecimen Repository for Reproductive Research (HS-15–00859) after appropriate approval was obtained unanimously from the Biorepository Ethics Committee. Supernumerary embryos were donated upon completion of IVF treated from USC Fertility. Patients were informed of the general conditions of the donation, as well as the objectives, and methodology of human embryo research. They were offered counselling and alternatives to donation, including discarding embryos and continued cryopreservation of embryos. Patients were informed that they would not benefit directly from the donation of embryos to research.

Human embryo culture and sample collection

University of Cambridge

A total of 8 donated two pronuclei stage human zygotes (day 1 post fertilization) from two patients were used for this study. Embryos were warmed and cultured according to the above regulations. Cryopreserved day 1 embryos were thawed with the Origio thaw kit (REF10984010A) following the manufacturer's instructions. Briefly, the Global Total human embryo culture medium (LifeGlobal group, H5GT-030) was incubated at 37°C and 5% CO_2 overnight before thawing. The next day, the straw containing the embryo was immersed in prewarmed (37°C) water for 1 min. The embryo was then transferred into vial 1 (5min), vial 2 (5 min), vial 3 (10 min), and finally into vial 4. Thawed embryos were finally incubated in drops of the pre-equilibrated Global Total human embryo culture medium under mineral oil (Irvine Scientific, 9305). Embryos were incubated for a total of 12 hrs overnight at 37°C and 5% CO_2 until the 2-cell stage The following day the zona pellucida of the 2-cell stage human embryos was removed by brief acidic Tyrode's solution treatment (Sigma, T1788).

Embryos were then bisected and single blastomeres transferred to M2 media before being washed and processed as above into 384-well PCR plates (ThermoFisher AB1384) in 1μl of pure water (Optima LC/MS Grade, Fisher Scientific W6500).

Of 8 two pronuclei zygote stage human embryos, 7 embryos developed to the 2-cell stage for sample collection and 5 were included in the final analysis.

California Institute of Technology

A total of 22 donated two pronuclei stage human zygotes (day 1 post fertilization) from 5 patients were used for this study. Cryopreserved day 1 embryos were warmed with the Embryo Thaw Media Kit following the manufacturer's instructions (Fujifilm Irvine Scientific, 90124). Briefly, the Continuous Single Culture-NX Complete medium (Fujifilm Irvine Scientific, 90168) was incubated at 37°C and 5% CO_2 overnight before thawing. The next day, the straw containing the embryo was defrosted at room temperature for 30 s and immersed in prewarmed (37 °C) water for 1 min until the ice melted. The embryo was then transferred into T-1 (5 min), T-2 (5 min) and T-3 (10 min) solutions for slow thawing, before being finally transferred to Multipurpose Handling Medium (Fujifilm Irvine Scientific, 90163) for recovery. Thawed embryos were then incubated in drops of pre-equilibrated Continuous Single Culture-NX Complete medium under mineral oil (Irvine Scientific, 9305). Embryos were incubated at 37°C, and 5% CO_2 for 6-12 hrs until they reached the 2-cell stage.

Assisted hatching was performed using laser pulses at 200 μs (Lykos laser: Hamilton Thorne, Beverly, MA, USA). Embryo Biopsy Medium (Irvine Scientific, 90103) was then used to separate the blastomeres from each other, followed by gentle pipetting of the embryo to remove it from the zona pellucida and isolate individual sister blastomeres. Blastomeres were then washed and processed as above into 384-well PCR plates in 1μl of pure water.

Of 22 two pronuclei zygote human embryos, 20 embryos developed to the 2-cell stage for sample collection and 8 were included in the final analysis.

Human stem cell culture and sample collection

The use of human ESCs (hESCs) was approved by the UK Stem Cell Bank Steering Committee and experiments complied with the UK Code of Practice for the Use of Human Stem Cell Lines. RUES2 hESCs (kindly provided by Ali Brivanlou) were used as carrier samples for SCoPE2. All cells were routinely tested for mycoplasma contamination.

RUES2 hESCs were cultured in a humidified incubator at 37°C and 5% CO_2 in mTeSR1 (StemCell Technologies, 85850) on growth factor-reduced Matrigel-coated (Corning, 353046). For Matrigel coating, plates were incubated with 0.16mg/ml Matrigel in DMEM/F12 (Gibco, 21331020) at 37°C for 1 hour. Media was changed daily.

hESCs were routinely passaged every 4–5 days by dissociating in Accutase (ThermoFisher Scientific, A1110501) for 3 minutes at 37°C. Cells were collected in DMEM/F12 and centrifuged for 3 minutes at 1000 rpm before being re-plated in mTesR1 medium supplemented with 10μM ROCK inhibitor Y-27632 (StemCell Technologies, 72304) for 24 hours.

For sample collection, cells were dissociated as above for routine passage. RUES2 hESCs were resuspended in PBS. Cells were pelleted by centrifugation for 4 minutes at 1200 rpm before a second PBS wash. Cells were resuspended in pure water at a density of 2000 cells/ul. 200,000–300,000 cells total were collected in 0.2ml PCR tubes and stored at -80°C.

METHOD DETAILS

Single-cell sample collection

The zona pellucida was removed prior to blastomere separation by brief acidic Tyrode's solution treatment (Sigma, T1788), followed by washes in M2 media. Embryos were then transferred to 35mm petri dishes (Corning, 351008) coated in 1% agarose and covered with M2 media. Blastomeres were separated from each other using a thin glass capillary and transferred immediately to M2 medium. Separation took up to 1 min and had a survival rate greater than 80%. Zygotes were split in a similar manner to give rise to two intact split halves. Zygotes were split meridionally in alignment with the animal-vegetal axis as defined by the position of the polar body. After the embryos had been split, individual blastomeres or zygote halves were washed through 7-10 washes of PBS (Life Technologies, 10010056) followed by 5 washes in pure water (Optima LC/MS Grade, Fisher Scientific, W6500), before being finally resuspended in 1μl of water and transferred to individual wells of a 384 well plate (ThermoFisher, AB1384), on a cold block. In order to minimize sample contamination all surfaces were cleaned and filter tips used. Wash drops were not reused more than 8 times and were changed if a blastomere lysed. Two different glass pipettes were used for the PBS and water washes to prevent carry over. In each experiment, sample collection took up to 1 hr and plates were subsequently sealed with foil (ThermoFisher, AB0626). The second polar body detached during separation and washes in the majority of embryos, but the identity of the blastomere with the polar body and whether the polar body remained attached or detached was annotated.

For PCNA live imaging experiments, zygotes were recovered as described above and microinjected. Following microinjection, embryos were cultured in KSOM media (Merck, MR-106-D) under mineral oil (Biocare Europe, 9305) at 5% CO_2, and 37°C overnight and allowed to cleave to the 2-cell stage. Prior to imaging, 2-cell embryos were split as above and transferred to an imaging dish. In experiments where further culture was required following imaging, split embryos were transferred to Global Total culture medium (LifeGlobal group, H5GT-030) under mineral oil at 5% CO_2, and 37°C, for 72 hrs.

For split embryo culture to the blastocyst stage, 2-cell stage embryos were split as above and single blastomeres cultured in drops of Global Total culture medium[90] under mineral oil at 5% CO_2, and 37°C, for 72 hrs.

For knockdown experiments, zygote or 2-cell stage embryos were recovered as described above, injected and cultured in KSOM media under mineral oil at 5% CO_2, and 37°C, until the required stage.

In vitro fertilization (IVF) and fertilization cone labelling

Following superovulation as described above, MII oocytes were recovered from the oviducts at 15 hrs post-hCG. Cumulus cells were removed by exposure to 200 IU/ml of hyaluronidase and oocytes were collected in CARD medium (Kyudo, KYD-005-EX). In parallel the cauda epididymis was recovered from culled males and the sperm extracted in CARD fertiup medium (Kyudo, KYD-005-EX). Following a 90 min capacitation at 5% CO_2, and 37°C, motile sperm were combined with the oocytes for IVF and kept at 5% CO_2, and 37°C for 2 hrs.

After IVF, the oocytes were cleaned of sperm and washed in M2 medium, and fertilized oocytes with a visible fertilization cone were collected. Fertilized oocytes were then transferred to a micromanipulator (Narishige) for the addition of a fluorescent microbead (approximately 6μm diameter, Polysciences, 18141) to the fertilization cone. A hole was manually made in the zona pellucida overlying the cone with a Piezo drive unit (Prime Tech) and the bead was pressed onto the cell membrane of the cone. Fluorescent (FITC labelled) microbeads were pre-incubated in M2 medium containing 500μg/ml phytohaemagglutinin (Sigma-Aldrich, L8754) overnight to allow for adhesion to the cell membrane.

For zygote splitting, labelled embryos were incubated in Advanced KSOM medium (SigmaMillipore, MR-101-D) from 3 hrs at 5% CO_2, and 37°C to the pronuclei stage, after which they were washed into M2 medium and the zona pellucida was removed by brief exposure to acidic Tyrode's solution as described above. Zygotes were then split meridionally, using the second polar body and the microbead as landmarks to orient the plane of splitting. Zygote halves were then collected as described above, annotating which half had the microbead attached. The bead fell off during the process of splitting in some cases. Furthermore, to ensure the microbead did not impact mass spectrometry analysis, sample sets were centrifuged following lysis, TMT labelling and sample pooling.

For split embryo culture experiments, labelled zygotes were incubated overnight in KSOM medium at 5% CO_2, and 37°C to the 2-cell stage. The zona pellucida was removed as described above and split sister blastomeres individually cultured to the blastocyst stage as above, annotating which sister had the bead attached.

Parthenogenetic activation of oocytes

MII oocytes were recovered as described above and activated in M2 medium with 10 mM $SrCl_2$ (Sigma, 439665) for 2.5 hrs at 5% CO_2, and 37°C. Parthenogenetically activated oocytes were then washed and cultured in KSOM media under mineral oil at 5% CO_2, and 37°C, until the 2-cell stage, after which they were split and collected as described above.

dsRNA and mRNA synthesis

The mCherry sequence was amplified via PCR from the pRN3P-H2B-mCherry vector and cloned into the pRN3p vector via EcoRI/BamHI digestion (ThermoFisher, FD0054 and FD0274) and T4 ligation (New England Biolabs, M0202S). pRN3P-mCherry was linearized using KpnI (New England Biolabs, R3142S). *In vitro* transcription was carried out using the mMessage mMachine T3 kit (Thermo Fisher, AM1348) and RNA purified via lithium chloride precipitation, according to the manufacturer's instructions.

pRN3P-Gap43-RFP and pRN3P-PCNA-Clover were linearized using SfiI (ThermoFisher, FD1824) and mRNA synthesized via in vitro transcription using T3 as above.

dsRNAs of 350-500bp length, were designed using the E-RNAi platform[91] and amplified from mouse liver cDNA. *In vitro* transcription was carried out using the MEGAscript T7 kit (Thermo Fisher, AM1334) and purified via lithium chloride precipitation, according to the manufacturer's instructions. Primers used for dsRNA synthesis are listed in Table S6.

Microinjection

Injection was performed as previously described.[73] Briefly, embryos were placed in a depression on a glass slide in M2 medium covered with mineral oil.Microinjection was performed using an Eppendorf Femtojet Microinjector with negative capacitance to facilitate membrane entry. Synthetic mCherry mRNA and Gap43-RFP were injected at a concentration of 200 ng/μl. For PCNA live imaging experiments, mRNA was injected at 100 ng/μl.[78] For knockdown experiments dsRNAs were injected at a concentration of 1000 ng/μl.

qRT-PCR

RNA was collected from embryos at 48 hrs post-injection, using the Arcturus PicoPure RNA isolation kit (Arcturus Bioscience, KIT0204), according to the manufacturer's instructions. Quantitative reverse transcriptase polymerase chain reaction (qRT-PCR) was performed using a StepOne Plus Real-time PCR machine (Applied Biosystem) and the Power SYBR Green RNA-to-CT 1-Step Kit (Life Technologies, 4389986). Relative mRNA expression levels of genes of interest were calculated using the ddCT method, with normalization to Gapdh. The primers used for qRT-PCR are listed in Table S6.

Immunofluorescence and confocal imaging

Blastocyst or 8-cell stage embryos were fixed in 4% PFA for 20 min at room temperature, and then washed through PBST (0.1% Tween 20 (Sigma Aldrich) in PBS) three times. Embryos were then permeabilized in 0.5% Triton X-100 (Sigma Aldrich) in PBS for 20 min at room temperature and washed through PBST again, before being transferred to blocking buffer (3% bovine serum albumin (Sigma Aldrich) in PBST) for 3 hrs at 4°C. Samples were then incubated with primary antibody mixes (diluted in blocking buffer) overnight at 4 °C. The next day, embryos were washed through PBST and incubated in secondary antibody mixes (1:500 in blocking buffer) with DAPI (Life Technologies, D3571, 1:1000 dilution, in PBST) for 2 hrs at room temperature. Finally, samples were washed through PBST following incubation with secondary antibodies and then imaged. Imaging was carried out on a SP5 or SP8 scanning confocal microscope (Leica) using the 63X or 40X oil objective.

Primary antibodies used: goat monoclonal anti Sox17 (R&D Systems, af1924, 1:200), mouse monoclonal anti Cdx2 (Launch Diagnostics, MU392-UC (Biogenex), 1:200), rabbit anti-Nanog (Abcam ab80892, 1:200) and rabbit anti RFP (Rockland, 600-401-379, 1:500).

Secondary antibodies used: Alexa Fluor 488 Donkey anti-Mouse, (ThermoFisher Scientific, A21202); Alexa Fluor 568 Donkey anti-Rabbit (ThermoFisher Scientific, A10042) and Alexa Fluor 647 Donkey anti-Goat (ThermoFisher Scientific, A21447). All secondaries were used at a 1:400 dilution.

Live Imaging

4-cell stage classification: Live imaging was performed with a SP5 scanning confocal microscope (Leica) using the 63x oil objective. 2- to 4-cell mouse embryos were imaged on glass-bottom dishes (MatTek, P35G-1.5-14-C) within a nylon mesh (Plastok) in KSOM media under mineral oil and kept in a humidified chamber at 5% CO_2, and 37°C throughout imaging. Images were captured every 15 mins with a z-step size of 5μm. Time lapse recordings were processed with Fiji software to assess division order, division timing and division pattern.

PCNA cell cycle assessment: Imaging was performed with a spinning disk confocal microscope (3i Intelligent Imaging Innovations) using the 63x oil objective, from 36 to 46 hrs post-hCG during the transition from S to G2 phase. Single blastomeres from split 2-cell embryos were imaged on glass bottom dishes, within a nylon mesh in KSOM media under mineral oil, at 5% CO_2, and 37°C. The imaging interval was 15 mins and the z-step size 5μm. After imaging a total of 30 single 2-cell stage blastomeres (15 split embryos) were collected for subsequent MS analysis as above. In a separate set of experiments blastomeres were allowed to undergo the second cleavage division during imaging and then removed from the imaging chamber and cultured to the blastocyst stage. Images were exported from SlideBook (3i Intelligent Imaging Innovations) and subsequently processed with Fiji software to assess S phase exit and division order when possible.

Mouse stem cell culture and sample collection

CAG-GFP/tetO-H2B-mCherry mouse embryonic stem cells (ESCs) were used as carrier samples for the SCoPE2. Cells were cultured on gelatin coated plates at 5% CO2, and 37°C in N2B27 2iLIF media. N2B27 2iLIF was comprised of 50% Neurobasal-A (Gibco, 10888022), 50% DMEM/F-12 (Gibco, 21331020), 0.5% N2 (in-house), 1% B27 (Gibco, 10889038), 2mM GlutaMAX (Gibco, 35050038), 0.1mM 2-mercaptoethanol (Gibco, 31350010) and 1% penicillin/streptomycin (Gibco, 15140122), with 3mM CHIR99021 (Cambridge Stem Cell Institute), 1mM PD0325901 (Cambridge Stem Cell Institute) and 10 ng ml-1 leukaemia inhibitory factor (Cambridge Stem Cell Institute) supplemented.

To induce H2B-mCherry expression, CAG-GFP/tetO-H2B-mCherry ESCs were treated with doxycycline (1 mg/mL) (Sigma-Aldrich, D9891-5G) for 6 hrs prior to collection.

ESCs were routinely passaged at 70% confluency following trypsinisation (Trypsin-EDTA 0.05%, Life Technologies, 25300054) for 4 minutes at 37°C. Feeder cell media was added to terminate the trypsinization and cells were dissociated by gentle pipetting and centrifuged for 4 minutes at 1000 rpm, before being re-plated at a 1:10 or 1:20 dilution. Feeder cell medium contained Dulbecco's modified essential medium (Gibco, 41966052), 15% fetal bovine serum (Cambridge Stem Cell Institute), 1mM sodium pyruvate, 2mM GlutaMAX, 1% MEM non-essential amino acids (Gibco, 11140035), 0.1mM 2-mercaptoethanol and 1% penicillin/streptomycin. Cells were routinely tested for mycoplasma contamination.

For sample collection, cells were trypsinized as above, and resuspended in PBS (Life Technologies, 10010056). The cells were then pelleted by centrifugation for 4 minutes at 1000 rpm before a second PBS wash. A haemocytometer was then used to estimate cell density and cells were pelleted as above, before being finally resuspended in pure water at a density of 2000 cells/ul. 200,000-300,000 cells total were collected in 0.2ml PCR tubes (Starlab, A1402-3700) and stored at -80°C.

Mass spectrometry (MS) sample preparation

Northeastern University: SCoPE2 and pSCoPE sample preparation

Isobaric carrier & reference: Sample preparation and analysis was performed as described by Petelski et al.[40] Briefly, mouse ESCs at a density of 2,000 cells/μl in 100μl water were lysed through the mPOP method (frozen cells were subjected to a rapid heat cycle of 90°C for 10 minutes, and then were cooled to 12°C).[40,41] Trypsin Gold (TG, Thermo) and triethylammonium bicarbonate (TEAB, pH = 8, Sigma) were added to the cell lysate to final concentrations of 10 ng/μl and 100 mM, respectively. The sample, once mixed with TG and TEAB, was subjected to 37°C overnight (16–18 hours) to digest proteins into peptides. To ensure adequate miscleavage rate (<20%), a small amount (1μl) of the cell digest was evaluated via LC-MS/MS. The cell digest was split into two samples, one for the carrier and the other for the reference. The carrier was labelled with TMT 126 and the reference was labelled with TMT 127N, with the labelling reaction proceeding for 1 hour. The reaction was quenched with 1% hydroxylamine (HA) for 30 minutes. Labelled material was then evaluated via LC-MS/MS for labelling efficiency (> 99%). Carrier and reference materials were kept frozen -80°C until needed for multiplexing with single cells.

Single blastomere cells and zygote halves: Frozen blastomeres that were collected in a 384-well plate were lysed by rapidly heating in a thermocycler to 90°C for 10 minutes and then cooled to 12°C. To each well (with a single blastomere or a water serving as the control), TG and TEAB were added to the cell lysate to final concentrations of 10 ng/μl and 100 mM, respectively. The plate was then subjected to 37°C for three hours. Each well then received 0.5μl of selected TMT reagents and the plate was incubated at room temperature for 1 hour. The labelling reaction was quenched with 0.5μl of 1% HA at room temperature for 30 minutes. Single blastomeres were then combined with 200 carrier and 5 reference cells to form a TMT set (Figure S1B). Each TMT set was dried down and resuspended in 1.1 μl of HPLC-grade water.

Sample preparation for label-free mass-spec single-cell proteomics: A total of eight 2-cell stage human embryos were used for label-free mass-spectrometry analysis. Frozen blastomeres that were collected in a 384-well plate were lysed by rapidly heating to 90°C for 10 minutes and then cooling to 12°C. To each well (with a single blastomere or a water serving as the control), TG and TEAB were added to the cell lysate to final concentrations of 10 ng/μl and 100 mM, respectively. The plate was then kept at 37°C for 3 hours to facilitate protein digestion. Each blastomere was dried down in a speed-vac and resuspended in 1.1 μl of HPLC-grade water for subsequent mass-spectrometry acquisition.

California Institute of Technology

SCOPE2 protocol for single cell proteomics: Cells/cell halves were lysed via Minimal ProteOmic sample Preparation (mPOP) method.[40] Briefly, the frozen cells in 384 well plates were quickly heated to 90°C for 10 min to rupture cells and quickly cooled down to 12°C. A digestion mix containing 25 ng/μl Trypsin Gold (Promega) and 250 mM Triethylammonium bicarbonate (TEAB, Thermo Scientific) was made during the lysis. After lysis, the plate was sonicated in a water-bath sonicater for 5 min, and was briefly spun down before digestion mix was added. 0.5 μl of the digestion mix was added into each well containing approximately 1 μl lysate. The final concentration of the Trypsin Gold and TEAB was 8.3 ng/μl and 83.3 mM, respectively. The digestion was allowed under 37°C for 3 hr, and the lid temperature was set at 52°C. Again, the plate was briefly spun down before further processing. At the same time, aliquots of 0.2 mg TMT 18-plex reagents (Thermo Scientific) were dissolved using 21.6 μl of anhydrous acetonitrile (Sigma-Aldrich) to make a 22 mM stock. 0.5 μl of 22 mM TMT reagent was added into each well,and the reaction mix was incubated at room temperature for 1 hr. After reaction, 0.5 μl of 1% hydroxylamine (Thermo Scientific) was added to quench the reaction, and the quenching reaction was allowed for 1 hr. After quenching, all the samples in the same TMT set were carefully combined and directly transferred to a glass insert of an autosampler vial. 5 μl of anhydrous acetonitrile was passed through the wells to rinse any leftover peptide for two times, and all the rinsing solutions were combined with the sample. The sample was then dried down using a CentriVap (LabConco) and was stored at -80°C until LC-MS/MS analysis.

Mass spectrometry acquisition methods

Northeastern University

TMT sets of single blastomeres were analyzed according to the SCoPE2 protocol guidelines. Specifically, 1 μl out of 1.2 μl of each SCoPE2 pooled sample was loaded onto a 25 cm × 75 1 μm IonOpticks Aurora Series UHPLC column (AUR2-25075C18A). Buffer A

was 0.1% formic acid in water and buffer B was 0.1% formic acid in 80% acetonitrile / 20% water. A constant flow rate of 200 nl/min was used throughout sample loading and separation. Samples were loaded onto the column for 20 min at 1% B buffer, then ramped to 5% B buffer over 2 min. The active gradient then ramped from 5% B buffer to 25% B buffer over 53 min. The gradient then ramped to 95% B buffer over 2 min and stayed at that level for 3 min. The gradient then dropped to 1% B buffer over 0.1 min and stayed at that level for 4.9 min. The total run time of each sample took 95 minutes total. All samples were analyzed by a Thermo Scientific Q-Exactive mass spectrometer from minutes 20 to 95 of the LC loading and separation process. Electrospray voltage was set to 2200 V and applied at the end of the analytical column. To reduce atmospheric background ions and enhance the peptide signal-to-noise ratio, an Active Background Ion Reduction Device (ABIRD, by ESI Source Solutions, LLC, Woburn, MA, USA) was used at the nanospray interface. The temperature of the ion transfer tube was 250 °C, and the S-lens RF level was set to 80.

California Institute of Technology

The sample in the autosampler vial was dissolved in 3 μl of LC-MS grade water and sonicated in a water-bath sonicater for 5 min. The vial was briefly centrifuged and transferred to the autosampler. The LC-MS/MS analysis was performed using a Thermo Eclipse Tribrid Mass Spectrometer coupled with a Thermo Vanquish Neo UHPLC system. The samples were analyzed on an Aurora Ultimate TS25 C18 column (25 cm x 75 μm, Ionopticks). Buffer A was 2% acetonitrile, and 0.2% formic acid in water, and Buffer B was 80% acetonitrile, and 0.2% formic acid in water. The gradient was 3% B for 1 min, 3-19% B for 54 min, 19-29% B for 21 min, 29-41% B for 15 min, 41-95% B for 1 min, and 95% B for 8 min. The flow rate was kept as 220 nl/min. The spray voltage was 1600V in positive mode, and the ion transfer tube temperature was kept at 300°C. MS1 scan resolution was set at 60000, and scan range was 375-1200. RF lens was set at 50%. The AGC target for MS1 was 300%, and the max injection time for both MS1 and MS2 was switched to auto mode. Intensity threshold for MS2 acquisition was 5.0e3, and dynamic exclusion was set to 45s. The isolation window for MS2 acquisition was 0.8 Th, and the peptides were fragmented using HCD with 35% NCE collision energy. The MS2 spectrum was acquired on orbitrap with 50000 resolution with the first mass as 120 Th. The AGC target for MS2 was 200%. The cycle time for duty cycles was 3 seconds.

Analysis of raw SCoPE2 and pSCoPE MS Data

Northeastern University

Raw data were searched by MaxQuant (version 1.6.17) against a protein sequence database including all entries from the mouse or human SwissProt database (depending on which samples were being analyzed) and known contaminants such as human keratins and common lab contaminants (default MaxQuant contaminant list).

Within the MaxQuant search, we specified trypsin digestion and allowed for up to two missed cleavages for peptides having from 7 to 25 amino acids. Tandem mass tags (TMTPro 16plex) were specified as fixed modifications. Methionine oxidation (+ 15.99492 Da), and protein N-terminal acetylation (+ 42.01056 Da) were set as variable modifications. Second peptide identification was disabled. Calculate peak properties was enabled. All peptide spectrum matches (PSMs) and peptides found by MaxQuant were exported in the evidence.txt files. These evidence files were then analyzed together by DART-ID.[92] The data from the files processed from DART-ID[92] was then processed with the SCoPE2 pipeline[41] with minor modifications, with filtering parameters including PEP < 0.03 and PIF > 0.8. Reverse matches and contaminants were also removed.

SCoPE2 pipeline is available here: (https://zenodo.org/record/4339954#.YnHcYSfMLOQ)

The carrier and reference material in these experiments are clearly a different cell type from the single cells that we have processed. Obtaining a large enough number of blastomeres to use as carrier and reference material for all the SCoPE2 sets was not possible. Although the cell types are different, we were still able to sequence and quantify many peptides that were heavily enriched in the blastomeres as shown in Figure S4D. These peptides and the corresponding proteins include classical markers of blastomeres and are biologically relevant, as evidenced by our analyses of mouse ESCs carriers vs blastomeres. The protein differences associated with alpha-beta asymmetry are also observed in our label free DIA experiments that did not use a carrier, suggesting that the choice of carrier is unlikely to strongly influence our results.

California Institute of Technology

The acquired data was processed using Proteome Discoverer 3.0 (Thermo Scientific) coupled with Chimerys. The raw data was searched against the swissprot proteome acquired from UniprotKB for corresponding species. The precursor tolerance was set at 10 ppm, and the fragment tolerance was set at 0.02 Da. Up to two miscleavages were allowed in the search, and only peptides within 7-30 amino acids were considered in the search. TMTpro (+304.207 Da) on lysine and peptide N-terminal was added as fixed modification, and oxidation (+15.995 Da) on methionine was added as variable modification. Carbamidomethylation (+57.021 Da) on cysteine was included as a fixed modification as requested by Chimerys search engine although no alkylation was made during the sample preparation. The search result was exported as excel files and was subjected to further analysis.

The search results were further analyzed using R code adopted from a previous publication.[41] Briefly, the data was normalized using median normalization, and imputed with a k-nearest-neighbor algorithm implemented by the impute.knn function from impute package in R. For each pair of cells/halves from the same embryo, the data was further normalized for each embryo. The data was further corrected by ComBat to mitigate the batch effect introduced by the TMT sets, and clusters were identified using a k-means clustering with k = 2. Differential expression analysis was performed between the two clusters using a Kruskal-Wallis test, and proteins with a p value < 0.05 were identified as significantly differential expressed proteins between the two clusters. All the plots were first made using in-house python scripts and then rendered using Adobe Illustrator.

Label-free DIA analysis and DIA-NN search parameters

Some human blastomeres were analyzed by label-free DIA using a 100 minute total gradient, of which 63 minutes were active (12 to 75 minutes). More specifically, the gradient used is as follows: 4% buffer B (minutes 0 - 11.5), 4%-8% buffer B (minutes 11.5 - 12), 8%-35% buffer B (minutes 12 - 75), 35%-95% buffer B (minutes 75-77), 95% buffer B (minutes 77 - 80), 95%-4% buffer B (minutes 80 - 80.1), 4% buffer B (minutes 80.1 - 100). Each duty cycle consisted of 2 MS1 windows with ranges from 480 - 1500 m/z. Each MS1 was followed by 3 MS2 windows spanning its m/z range (2x 1 MS1 full scan x 3 MS2 windows). The size of the 6 MS2 windows in each duty cycle were variable and were as follows: 480 - 530 m/z; 530 - 590 m/z; 590 - 650 m/z; 650 - 750 m/z; 750 - 1000 m/z; 1000 - 1500 m/z. Each MS1 and MS2 scan was conducted at 140k resolving power, $3x10^6$ AGC maximum, and 600 ms maximum injection time for both MS1 and MS2 scans.

Raw data was searched with DIA-NN (version 1.8)[93] against a protein sequence database that included entries from the human SwissProt database (SwissProt_human_09042017, containing 20,218 proteins). The fragment sizes were set from 200 - 1800 m/z, with N-terminal methionine excision enabled. We specified the search for trypsin digestion and set the maximum number of missed cleavages to 1. Scan window radius was set 1, while the peptide lengths were set at 7 - 30 amino acids.

QUANTIFICATION AND STATISTICAL ANALYSIS

Image analysis and statistics

Images were processed with Fiji software[88] (2012, https://imagej.net/software/fiji/) to assess cell number and lineage allocation. Cell numbers were counted manually, using the multi-point counter function.

The statistical test used is indicated in the corresponding figure legend. In all cases, the two-tailed version of the test was used. Normality of the data was assessed using the Shapiro Wilk test. Statistical analysis was performed using Prism software (version 8, GraphPad, https://www.graphpad.com/scientific-software/prism/).

K-means Clustering

To estimate the stability of the cell classification that was accomplished via k-means clustering, we computed the stability of cluster assignment. Through 200 iterations in which the starting cell centroid was changed for each cluster, we estimated the probability of cluster assignment for each. The overwhelming majority of cells have a high probability of landing in the same cluster consistently when initial conditions are changed. There are some blastomeres (n=9) that seem to exhibit unstable cluster assignment, which we have been unable to link to division order, division timing, or division pattern. For simplicity's sake, we arbitrarily termed these clusters as alpha and beta. The same approach was used for both the human blastomeres from 2-cell embryos and the cut zygotes data.

Determining differential proteins between alpha- and beta-cell types

Once cells were assigned to their respective classes via k-means clustering (k=2), we determined which proteins were significantly differentially abundant between the two groups of blastomeres using a series of Kruskal-Wallis tests (effectively a Mann-Whitney-Wilcoxon test). At least three observations per group were required for each protein. P values of the tested proteins were adjusted for multiple hypotheses through the BH method to estimate the false discovery rate (FDR). A threshold of 5% FDR was implemented as the cutoff for significance for all results.

From these analyses, we obtained a list of differentially abundant proteins in 2-cell embryos and used these proteins to plot two heatmaps in order to designate between the early and late 2-cell stages. The heat maps represent the proteins x blastomeres matrices. The columns of each heatmap were ordered by descending degree of asymmetry of sister blastomeres. The leftmost and rightmost columns correspond to blastomeres from the same embryo, a pattern that continues to the center of the heatmap.

Overall, 349 proteins that are distinguishing the alpha-beta clusters. Out of this list, 163 proteins were quantified in the mouse zygote data, which is 47% of the defined alpha-beta proteins.

Overall, we quantified an average of 3586 peptides mapping to 1043 proteins in the mouse blastomere samples, and a mean of 2895 peptides mapping to 759 proteins in the human blastomere samples.

Comparison between bulk stem cells and mouse blastomeres

Blastomere Peptide Enrichment

We plotted the reporter ion intensities (without any data processing) of a representative blastomere and its respective carrier on the log10 scale. In doing so, we find that some peptides are much more abundant in one blastomere as compared to a 200-cell sample. In order to find what biological processes are enriched generally across mouse blastomeres as compared to ESCs, we obtained the precursor ratios of each blastomere to each respective ESC carrier. Then, we took the median across all blastomere-ESC pairs to obtain the median ratio for each precursor. Then, these ratios were further collapsed to the protein level by taking the median across all peptides mapping to that protein. With this list, we were able to rank proteins from greatest to least ratios, then input this ranked list into GOrilla using "single ranked list of genes" mode. From this output, we find that protein transport and protein degradation are largely enriched in blastomeres.

Protein Set Enrichment Analysis (PSEA) for Alpha vs Beta Comparison

To determine which processes are differential between alpha- and beta- cell clusters, we first downloaded protein sets from MGI (MGI Data and Statistical Reports (jax.org)). These terms were filtered for proteins by Gene Symbols that were quantified in the mouse data. For each GO term, proteins by Gene Symbol that were associated with that GO term were collected into a single data frame. That data frame was further stratified into two groups: alpha- and beta- type. Each group was required to have greater than three observations. The two distributions per GO term were tested using the Kruskal Wallis test (effectively a Mann-Whitney-Wilcoxon test). P values of the tested GO terms were adjusted for multiple hypotheses, using the BH procedure to estimate the False Discovery Rate (FDR). GO terms were deemed significant if they passed the 5% FDR threshold.

For the mouse data, there were many GO terms that were significant (n = 2898 at 5% FDR, n = 1499 at 5% FDR and with greater than 2 proteins associated with the term). In order to make sense of all the terms, the data was stratified into themes of protein degradation, protein transport, translation, and metabolism through filtering of the names of the GO terms. These themes were further grouped into sub-themes in the same manner.

This approach was also used for the human 2-cell-stage data, using protein sets defined for human data.

Ribosomal Protein Analysis

For each ribosomal protein (RP) that was quantified, we used the Mann-Whitney-Wilcoxon test to understand whether the abundance of the particular RP was different between alpha and beta cells across all available mouse blastomeres (from early 2-cell to 4-cell stage). From these analyses, we found that eight RPs are significantly differential (q-value < 0.05). The distribution of these proteins' fold-changes between sister alpha and beta cells were plotted as boxplots at each stage.

Vegetal cell analysis

To identify whether alpha / beta polarization is associated with vegetal cell identity, we clustered 4-cell stage blastomeres with well differentiated alpha-beta character (alpha-beta fold change greater than 0.05 or less than -0.05) based on their relative protein levels, as shown in Figure 4F. As expected, the blastomeres clustered by alpha / beta polarization, and this clustering also portioned the vegetal cells. We evaluated the statistical significance of this portioning using the hypergeometric distribution to compute the cumulative probability (p-value) that the vegetal cells exhibit the observed association with alpha character or larger if sampled randomly.

Across the stages Analysis

To assess which biological processes are driving this trend, fold changes between sister blastomeres assigned to opposing classes were calculated for each protein. With these values, we sought to identify functionally related proteins that covary among the three stages using spearman correlation analysis. For this analysis, we looped through each protein or each protein set and correlated the stages (set to be numerical) to fold changes between alpha and beta blastomeres of normalized protein abundances. From each correlation, we also obtained a p-value. Protein sets were required to have more than two proteins and more than 50% of proteins quantified. These p-values were then corrected for multiple hypotheses.

Comparison between human and mouse 2-cell embryos

Pairwise Cell-to-Cell Correlation Heatmap

All proteins that were quantified in both datasets were used to calculate pairwise Spearman correlations between human and mouse blastomeres at the 2-cell stage. The heatmap of Spearman correlations was then plotted to have mouse blastomeres on the x-axis and human blastomeres on the y-axis. The human blastomeres are ordered in the same way as the dendrogram presented. The mouse blastomeres are clustered by their respective cluster-type, alpha or beta. We observe two distinct clusters, meaning that human 2-cell stage embryos also exhibit a similar proteome asymmetry.

Intersected Protein Set Heatmap

Protein sets that were found to be differentially abundant between alpha and beta cells in mouse were intersected with protein sets that were found to be differentially abundant between the respective two clusters. Both heatmaps were hierarchically clustered on the rows (protein sets) and blastomeres on the columns were clustered according to the cell classification via k-means clustering. Each tile in the heatmap represents the median value on the log2 scale of that particular protein set in a particular blastomere.

Cut zygotes analysis

Upon normalization and performing k-means clustering in the same manner as in the mouse and human data, all quantified proteins in the zygotes were used to perform principal component analysis. As zygote cutting may result in halves that are not exactly equal in volume, the peptide distribution of each sample (zygote half) was normalized for sample loading, thus accounting for any potential uneven sample distribution. This also aided the generation of one matrix of all samples to obtain relative protein quantitation. Each zygote half fell into a cluster opposite its partner half, which we simply termed in this case "Cluster 1" and "Cluster 2". The difference in the first principal component (PC1) values were taken for each zygote pair and plotted in a descending order as a bar plot. Then, protein fold changes between the partner cut pieces were calculated for each zygote (these values were calculated consistently by finding the difference between the zygote piece in Cluster 1 and in Cluster 2. These vectors of protein fold changes for each zygote were then correlated pairwise to protein fold changes of each mouse 2-cell stage blastomere (which were consistently calculated as

the difference between alpha and beta cells), resulting in a correlation matrix. These results were plotted as distributions per zygote, with the median of each distribution highlighted as a purple diamond (Figure 2E).

In order to see the overall correlation between the zygote and mouse 2-cell blastomeres, the median fold change of each protein was calculated across all samples in respective groups (zygotes and 2-cell embryos). With these two vectors, a scatterplot of mouse 2-cell embryos protein fold-changes was plotted against the zygote fold-changes. The correlation of these vectors was positive (with a value of 0.45) and was highly significant (p-value = 1.39×10^{-9}).

Split Blastomere Experiment Analysis

Each blastomere that was used for MS analysis was prepared in a similar manner as was described in section titled "sample preparation for label-free mass-spec single-cell proteomics" The MS acquisition was altered, so that peptides mapping to alpha-beta proteins were prioritized using prioritized SCoPE (pSCoPE),[76] which was set up as described below, broadly following figure S4 from Huffman et al.

Gas phase fractionation (intensity-based quintiles spanning: 450-550, 550-623, 623-694, 694-788,788-1436 m/z respectively) was carried out to generate an empirical library using 5x TMT labelled mouse ESC carrier-reference runs. Post-acquisition, the runs were searched alongside all previous single cell DDA runs using Spectronaut (version 16.1), the generated spectral library was filtered at 5% FDR.

Subsequently, a 1x TMT labelled carrier reference sample was analyzed in DIA mode (using method outlined in Supplementary Table 5 from 10) to record accurate retention times for precursors. The run was searched using Spectronaut (filtered at 1% FDR).

The inclusion list was generated using peptides confidently identified in the 1x run. Peptides were split into 3 tiers, the highest tier contained peptides belonging to alpha and beta proteins, while the following two tiers contained peptides split by intensity, confidence of identification and precursor ion fraction. The inclusion list is provided as a supplementary file.

Prioritization was implemented using MaxQuant.Live Version 2.2.011. Targeting parameters were the same as in Supplementary table S13 (Method 5) of Huffman et al.,[76] with the exception that survey scan life cycle was set to 1500ms, MS2 resolution was 70,000 and MS2 max injection time was 256ms.

The resulting data was searched using MaxQuant and then normalized as described previously in the section titled "analysis of raw SCoPE2 and pSCoPE MS Data", except that the final protein x samples matrix was normalized relative to the mean of all analyzed cells. Then, for each blastomere, the median abundance of alpha proteins was divided by the median abundance of beta proteins to estimate the alpha-beta fold change of the analyzed cell. By designating which proteins are alpha and which are beta from previous clustering the "likeness" or polarization of blastomeres could be calculated, with a higher median alpha protein level indicating alpha identity, and higher median beta protein level indicating beta identity. After calculating the alpha-beta protein fold change or alpha-beta likeness of a blastomere, it can be inferred that the cultured sister blastomere is of the opposite identity, as 2-cell stage sisters consistently separated into opposing clusters. Each blastomere's fold change was then plotted against the proportion of epiblast cells in resultant blastocyst from the sister cell that was cultured. An overall positive trend is observed in the data, Figure 4C. The distributions of alpha-beta fold changes were further analyzed by separating all blastomeres into two groups: (1) those whose sister blastomeres gave rise to blastocysts containing equal to or more than 4 epiblast cells and (2) those whose sister blastomeres gave rise to blastocysts with less than 4 epiblast cells, indicating the health of the embryo at this developmental stage.

Supplemental figures

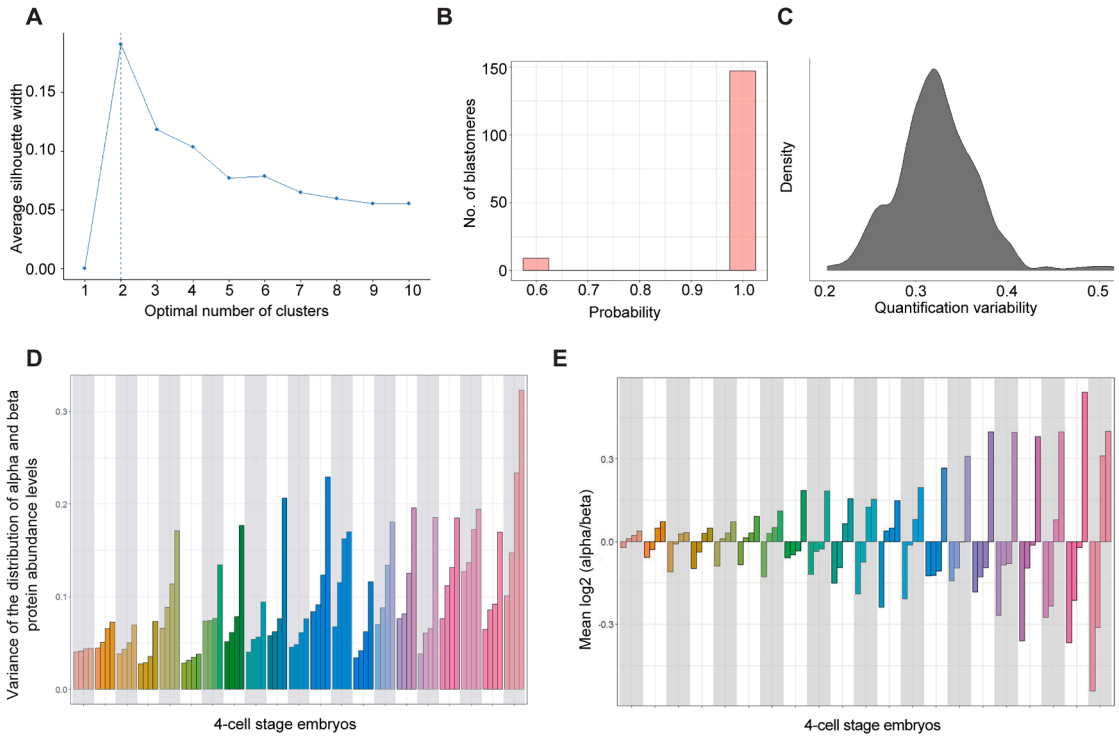

Figure S1. Data exploration, related to Figure 1

(A) Plot showing the number of clusters (k) plotted against the average silhouette width. In this case, k = 2 provides the best explanation for the data.

(B) Plot showing the probability of cells landing in the same cluster (alpha or beta) when changing the starting centroids in the k-means clustering approach 200 times to obtain vectors of cell cluster classification for each iteration. The majority of embryos consistently fall into the same cluster, indicating that the clustering approach is stable.

(C) Representative density plot showing quantitation variability for peptides mapping to the same protein in each mouse blastomere.

(D) Plot showing the variance in alpha-beta protein quantitation for each blastomere of 4-cell-stage embryos. The *y* axis shows the variance of alpha and beta protein abundances in each blastomere.

(E) Plot showing the variability in alpha-beta protein fold changes among sisters from each 4-cell-stage embryo. The *y* axis shows the fold change between the mean abundances of alpha and beta proteins in each blastomere.

In (D) and (E), each grouping of 4 blastomeres represents an embryo on the *x* axis, and all blastomeres that were part of the same embryo are colored in shades of the same color.

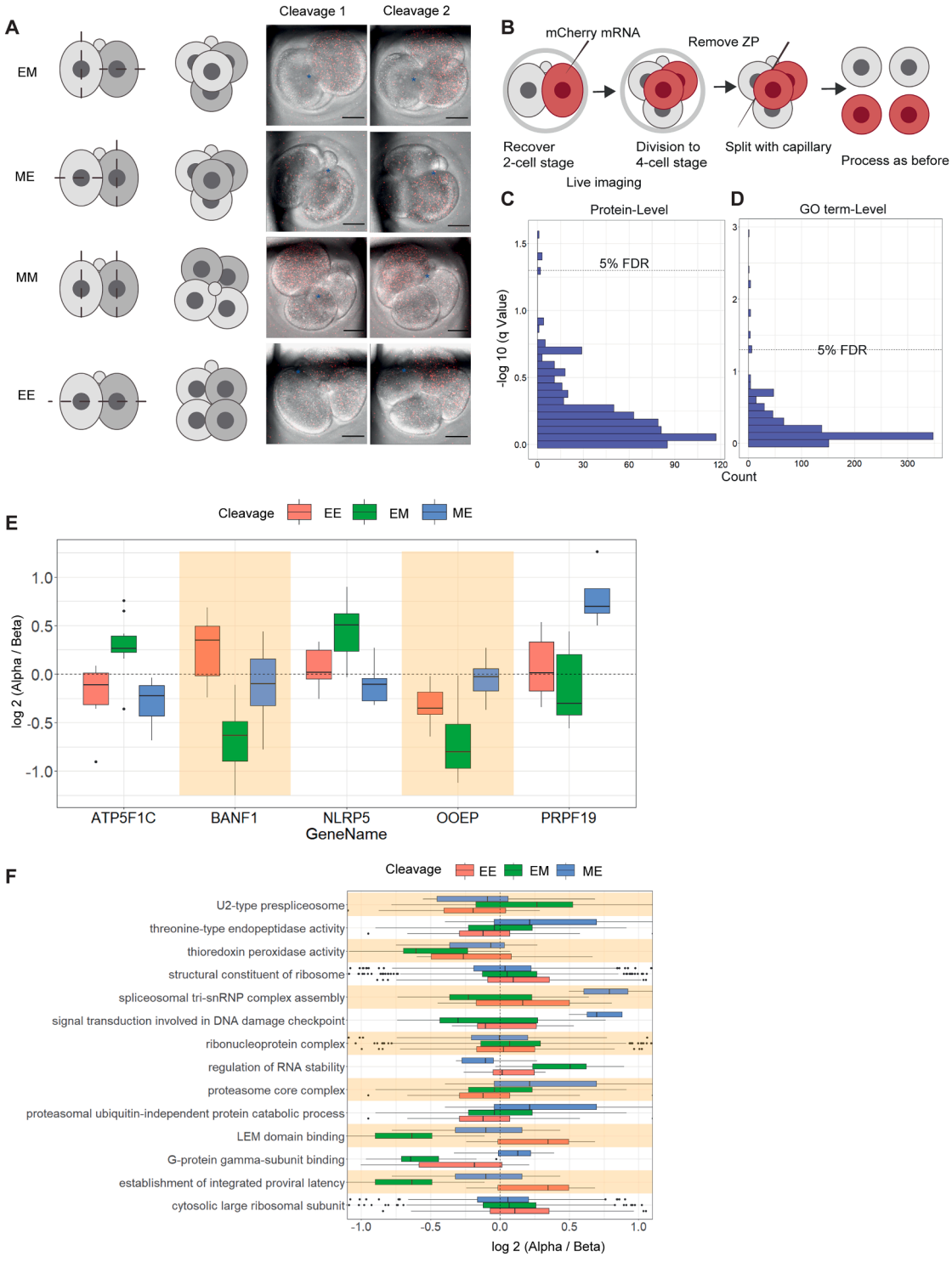

Figure S2. Cleavage pattern analysis between alpha and beta cells, related to Figure 1

(A) Schematic of division patterns from the 2- to 4-cell stage and representative stills from live imaging to classify division pattern. E denotes an equatorial division and M a meridional in relation to the animal-vegetal axis of the fertilized egg, with the first letter denoting the first cleavage and the second letter the second. ME, M-division followed by E-division; EM, E-division followed by M-division; MM, consecutive M-divisions; EE, consecutive E-divisions. The position of the PB is indicated with an asterisk. Scale bar, 20 μm.

(legend continued on next page)

(B) Schematic showing the experimental harvesting of single blastomeres from 4-cell-stage embryos, with classified division pattern and order. Division pattern and order were classified by live imaging, following injection of synthetic mCherry mRNA to label one of the two sisters at the 2-cell stage. After live imaging, the zona pellucida (ZP) was removed, and blastomeres were separated from each other and collected for SCoPE2.
(C and D) Plots showing the q value distributions for protein-level and GO term-level analyses. The dotted line indicates a q value of 0.05.
(E) Plot showing the fold changes for proteins within the 5% FDR threshold in determining differences between alpha and beta cell clusters among the cleavage patterns.
(F) Plot showing the fold changes for GO terms that passed the 5% FDR threshold in determining differences between alpha and beta cell clusters within the scope of cleavage patterns.

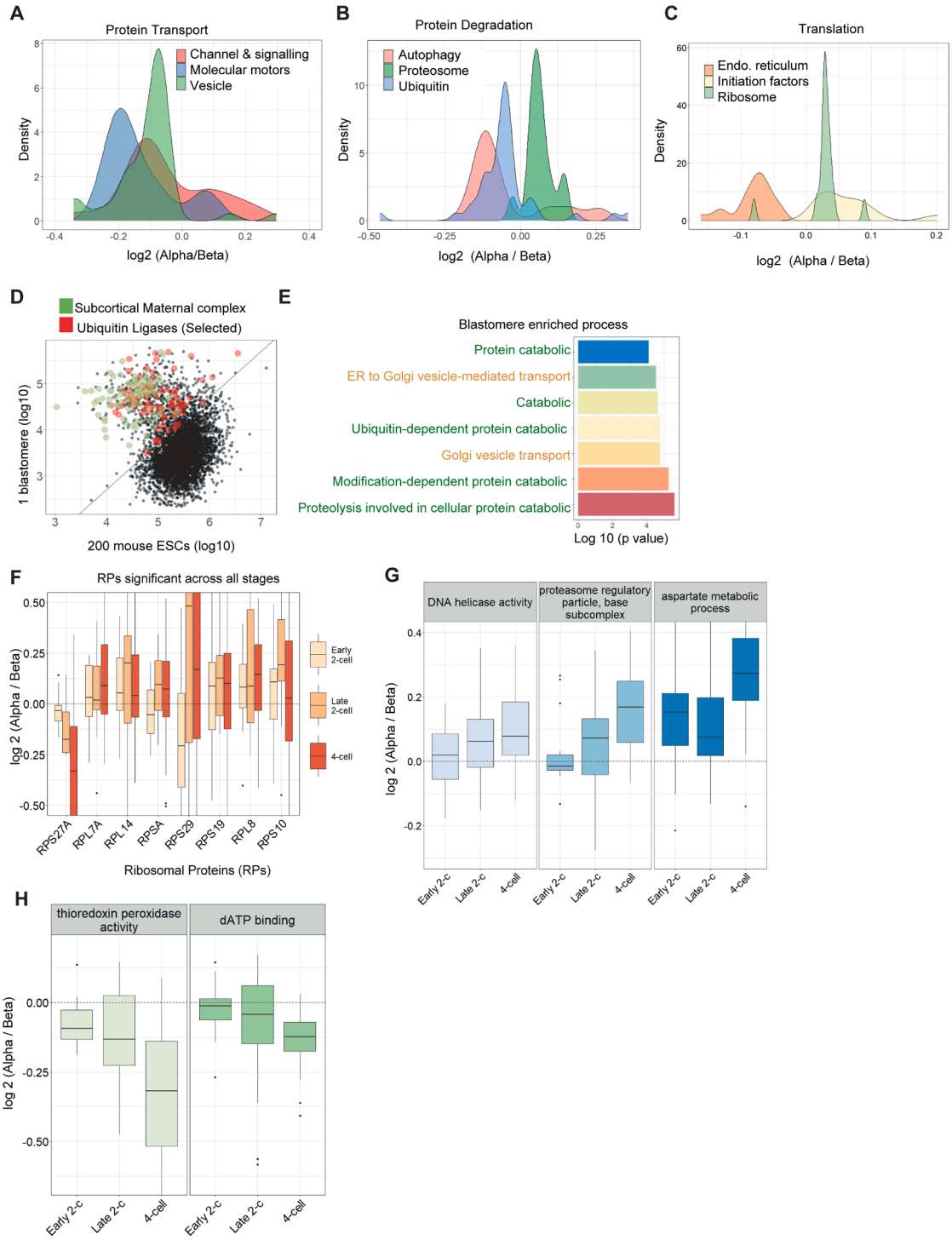

Figure S3. Differential biological processes between alpha and beta blastomeres and temporal overview of differences between alpha and beta cells, related to Figures 1 and 2

(A–C) Density plots showing the results of PSEA analysis, which revealed differential abundance of proteins related to specific biological processes between alpha and beta cell clusters, namely protein transport (A), protein transport (B), and protein translation (C).

(D) Scatterplot of raw reporter ion intensities from one representative blastomere versus 200 ESCs on the $\log_{10}$ scale. Green points correspond to peptides of proteins mapping to the subcortical maternal complex. Red points correspond to peptides of proteins mapping to ubiquitin ligases. The diagonal line represents the separation between the two clusters. Similar scatterplots were observed for blastomeres across all stages analyzed. Upon systematic analysis of all blastomeres in all stages, we found proteins involved in protein degradation and transport to be heavily enriched in blastomeres as compared with ESCs.

(legend continued on next page)

(E) Bar plot showing the *p* values of the topmost enriched processes in blastomeres relative to ESCs. Green font corresponds to protein degradation processes, while yellow font corresponds to protein transport processes.
(F) Boxplots illustrating the levels of significantly differential (1% FDR) ribosomal proteins (RPs) between alpha and beta cells. The color of the boxplots corresponds to the developmental stage. RPs were tested separately between alpha and beta cells and for each stage.
(G and H) Boxplots showing the correlation values of protein sets (by highest absolute correlation value) obtained from analysis across the stages to identify processes that are increasing in alpha or beta blastomeres, respectively.

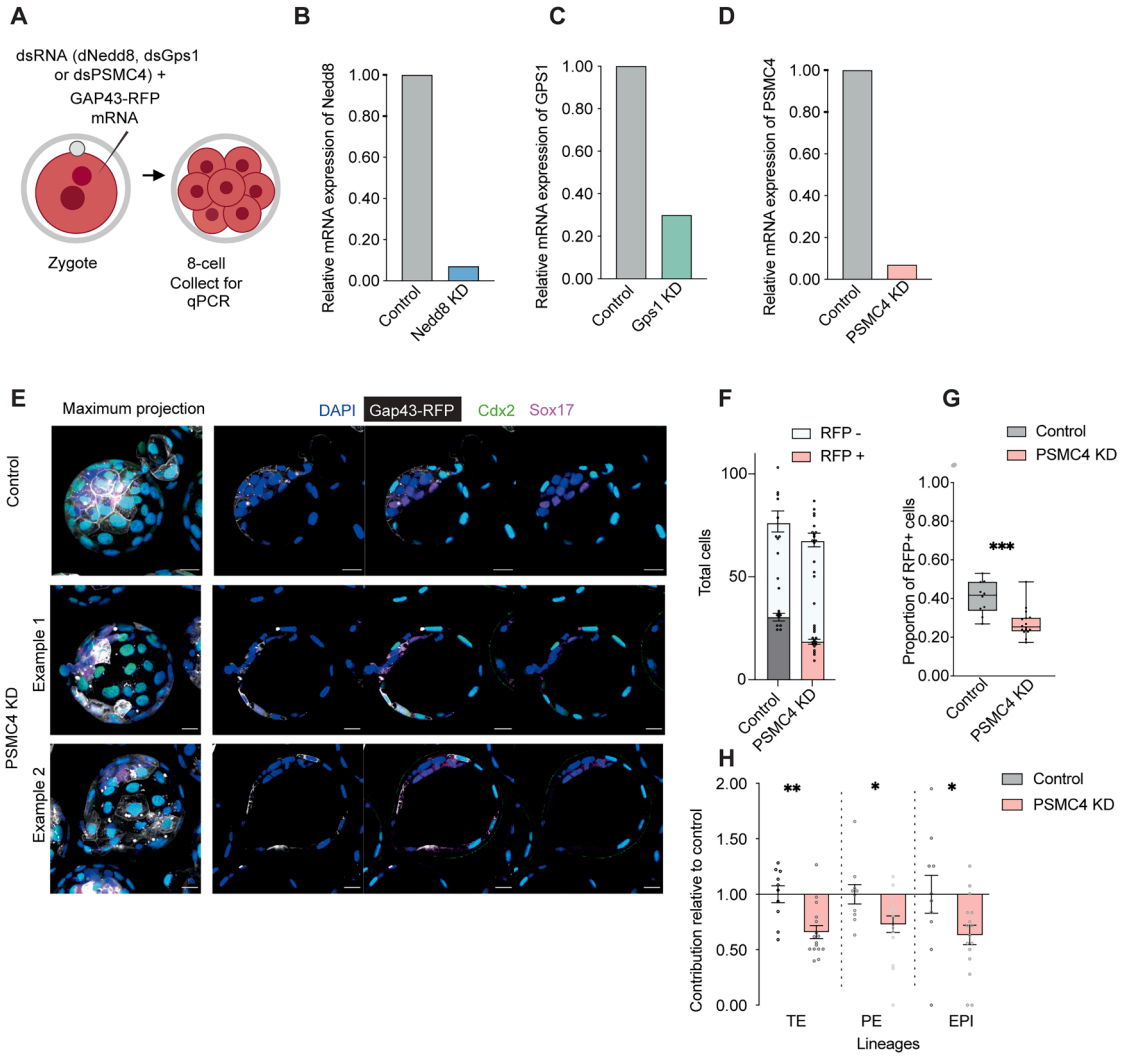

Figure S4. Validation of knockdown and assessment of knockdown of an alpha protein (PSMC4), related to Figure 3

(A) Schematic for validation of dsRNA-mediated knockdown. Embryos were injected with dsRNA targeting candidates (Nedd8, dsNedd8, Gps1, dsGps1, PSMC4, and dsPSMC4) or eGFP (control) and collected after 48 h for RT-qPCR at the 8-cell stage.

(B) Nedd8 mRNA expression was assessed relative to control embryos. Control, n = 14 embryos; dsNedd8, n = 14 embryos.

(C) Gps1 mRNA expression was assessed relative to control embryos. Control, n = 15 embryos; dsGps1, n = 15 embryos.

(D) PSMC4 mRNA expression was assessed relative to control embryos. Control, n = 14 embryos; dsPSMC4, n = 14 embryos.

(E) Representative images of control (ds-eGFP) and of dsPSMC4 blastocysts, following the same experimental design as Figure 3A. Scale bar, 20 μm.

(F) Bar chart showing the average total number of cells and the number of RFP-positive or -negative cells in control and dsPSMC4 late blastocysts.

(G) Boxplot showing the RFP-positive proportion of total cells in each blastocyst. Decreased contribution of dsPSMC4 cells can be seen. Mann-Whitney test, ***$p < 0.001$.

(H) Bar plot showing the contribution of RFP-positive cells to the trophectoderm (TE, Cdx2 positive), primitive endoderm (PE, Sox17 positive), and epiblast (EPI, double-negative), with dsPSMC4 contribution assessed relative to controls. dsPSMC4 cells show decreased contribution to all three lineages. Mann-Whitney test, *$p = 0.0449$ (PE), *$p = 0.0475$ (EPI), **$p < 0.0017$. Control, n = 10 embryos; dsPSMC4, n = 16 embryos.

Data are shown as mean ± SEM. For (F)–(H), data are shown as individual data points on a box and whiskers plot.

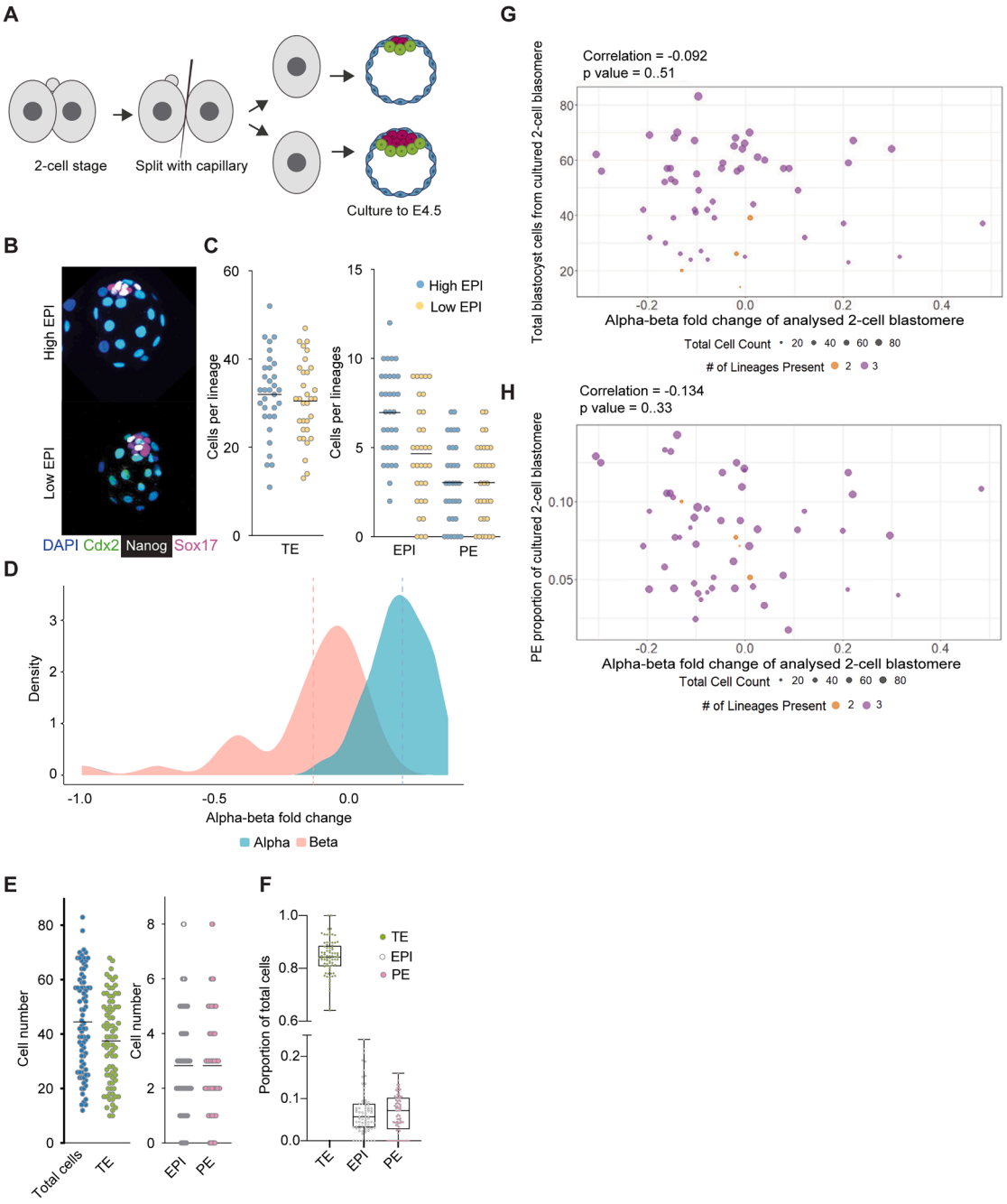

Figure S5. Sister 2-cell blastomeres show differences in their development, related to Figure 4

(A) Schematic of split embryo culture. 2-cell embryos were recovered and split before being cultured to the late blastocyst stage in pairs. Blastocysts were assessed for lineage marker expression.

(B) Representative images of a pair of twin blastocysts, showing one twin has more (high) or fewer (low) epiblast (EPI) cells. Images are maximum projections showing the composition of the ICM.

(C) Plots showing the number of cells in each lineage (trophectoderm [TE, Cdx2-positive], EPI [Nanog-positive], and primitive endoderm [PE, SOX17-positive]) for twin embryos classified as high or low EPI within the blastocyst pair. *n* = 32 pairs of blastocysts.

(D) Density plot showing the alpha-beta protein fold changes following global (across all embryos) normalization. The blastomere type ("alpha" or "beta") was defined by K-mean clustering following within-embryo normalization for the 2-cell-stage samples in which the proteomes of both sisters were analyzed. The alpha-beta fold change was then computed for each blastomere following normalization to the mean across all single 2-cell blastomeres rather than within each 2-cell embryo. Color indicates the clustering based on normalization within each embryo, while the alpha-beta protein fold change derived from normalizing across all blastomeres is shown on the *x* axis.

(legend continued on next page)

(E and F) Plots showing the cell number in each lineage and proportion of each lineage, respectively, in blastocysts from Figures 4A–4D. *n* = 81 embryos.
(G) Scatterplot of the total number of cells in each paired blastocyst versus the alpha-beta polarization of the sister cell analyzed by MS. No correlation is observed.
(H) Scatterplot of PE proportion in each paired blastocyst versus the alpha-beta polarization of the sister cell analyzed by MS. A negative correlation that is not statistically significant is observed.
In (G) and (H), circle size indicates the total number of cells in the imaged blastocyst, and circle color indicates the number of lineages present in each blastocyst.

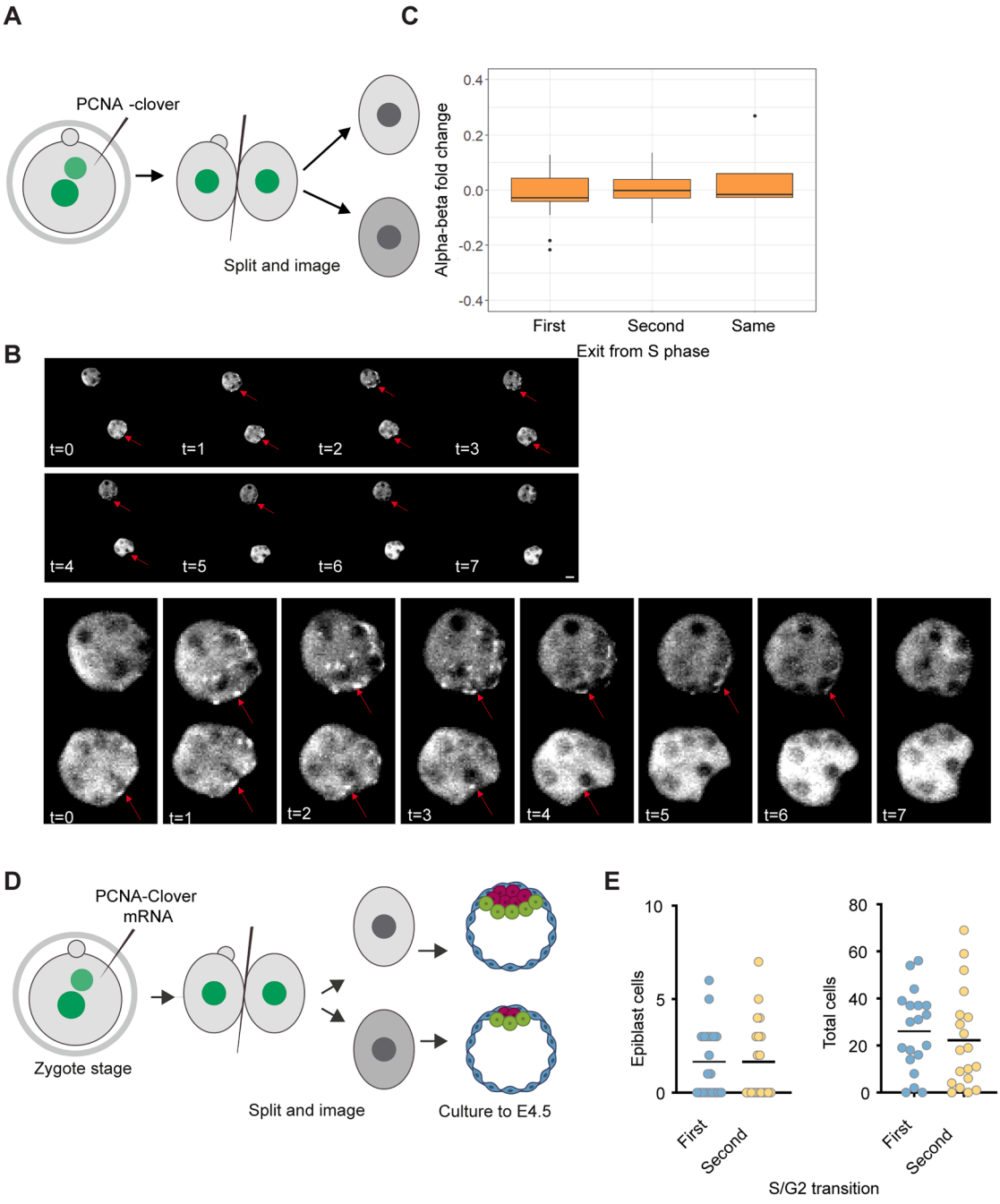

Figure S6. Alpha-beta polarization does not relate to cell cycle asynchrony as assessed by PCNA expression, related to Figure 4

(A) Schematic of cell cycle analysis by live imaging of embryos expressing PCNA-clover. Zygotes were injected with PCNA-clover mRNA and allowed to cleave to the 2-cell stage. 2-cell embryos were split and imaged from 36 to 46 h post hCG, during the transition from S to G2 phase, before being collected for single-cell proteomics.

(B) Representative still images of live imaging with PCNA-clover expression during the S/G2 transition. Red arrows indicate foci of PCNA-clover, which disappear as the cell enters G2. Magnified views are shown below. Time interval = 15 min. Scale bar, 10 μm.

(C) Boxplots of alpha-beta polarization (derived from normalization across all single blastomeres) as distributed between blastomeres that exited S phase either early or late. *n* = 30 blastomeres from 15 embryos.

(legend continued on next page)

(D) Schematic of cell cycle analysis by live imaging of embryos expressing PCNA-clover, followed by culture to the blastocyst stage. Zygotes were injected with PCNA-clover and imaged as in (A). Following live imaging, split embryos were cultured to the blastocyst stage, and lineage composition was assessed by immunofluorescence.

(E) Epiblast and total cell number in blastocysts do not show any relation to S/G2 transition. Live imaging was used to determine which sister had exited S phase/entered G2 first or second. *n* = 38 blastocysts from 19 2-cell-stage embryos.

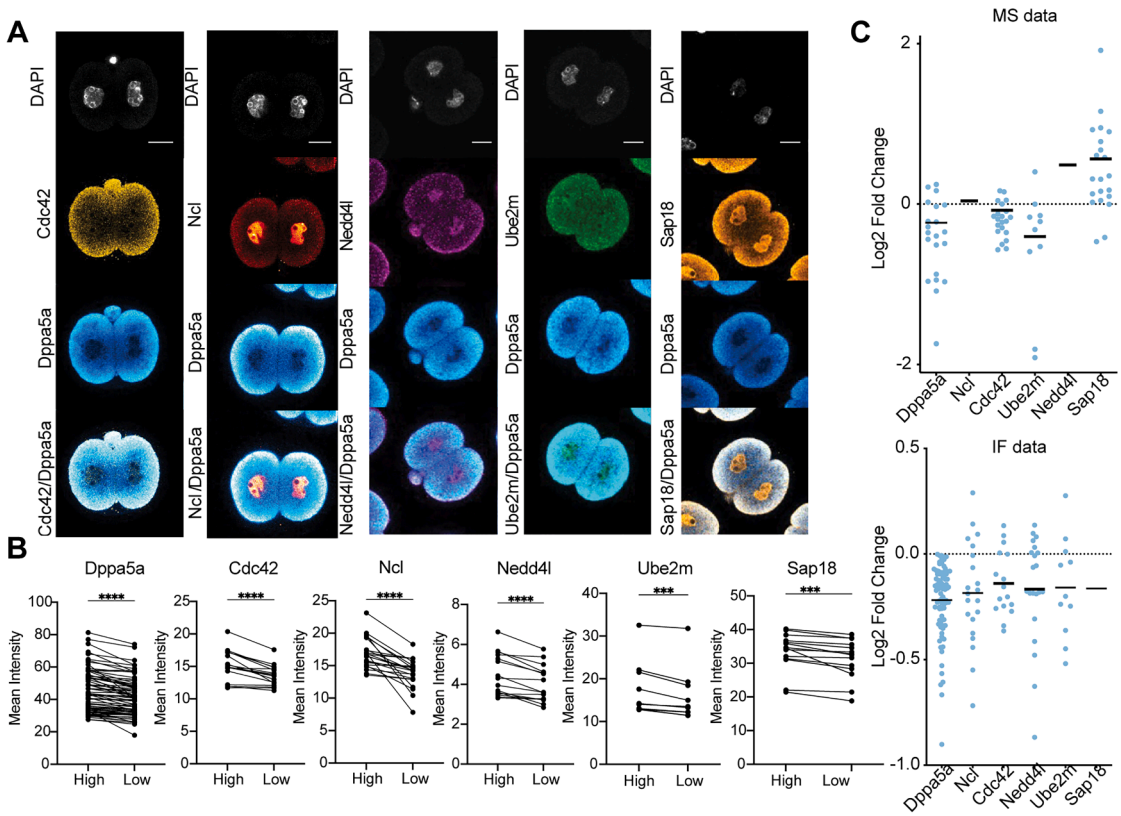

Figure S7. Immunofluorescence-based approach to assess proteome asymmetry, related to Figure 1

(A) Representative immunofluorescence staining of asymmetrically distributed proteins in late 2-cell-stage embryos, following fixation and labeling with the corresponding antibodies. Scale bars, 20 μm.

(B) Quantification of immunofluorescence signal intensity. Sister blastomeres were classified based on signal intensity as "high" or "low," as indicated on the *x* axis. Dppa5a, *n* = 81 embryos; Ncl, *n* = 23 embryos; Cdc42, *n* = 17 embryos; Nedd4l, *n* = 18 embryos; Ube2m, *n* = 11 embryos; Sap18, *n* = 14 embryos.

(C) Comparison of fold changes as quantified by mass spectrometry (MS) (top) and immunofluorescence (IF, bottom). For MS data, fold changes were calculated between alpha and beta cells as defined by clustering. For IF data, Dppa5a signal intensity was used to classify sisters, and fold changes were calculated between Dppa5a-high and Dppa5a-low sisters. Overall, IF was unable to detect intensity differences that corresponded to the MS data.